Cell Reports

Article

Landscape and age dynamics of immune cells in the Egyptian rousette bat

Graphical abstract

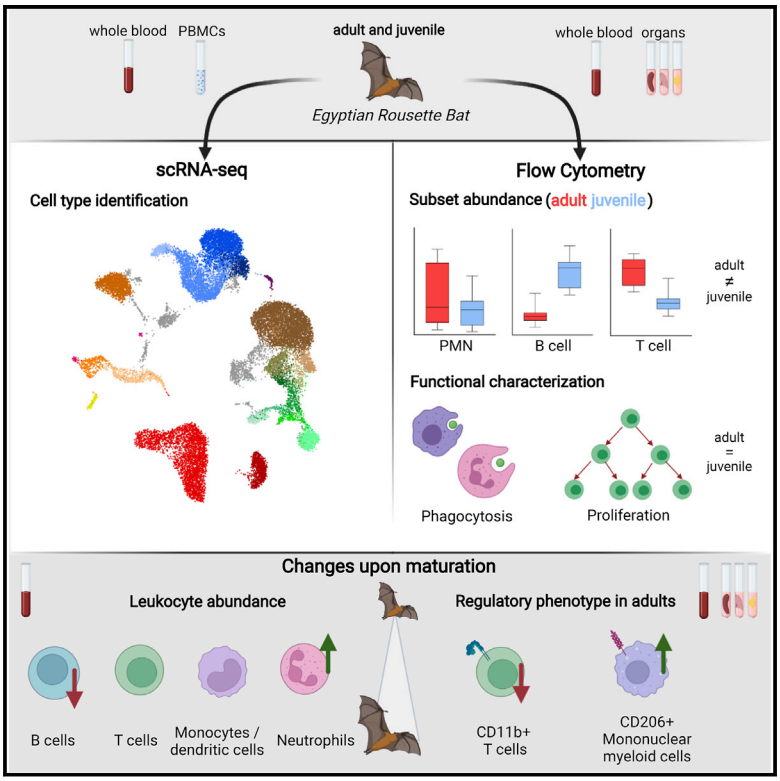

Highlights

- 22 unique leukocyte transcriptional subsets in Egyptian rousette bat (ERB) circulation
- Neutrophils, CD3$^+$ T cells, and CD206$^+$ mononuclear myeloid cells enriched in adult ERBs
- CD79a$^+$ B cells and CD11b$^+$ T cells more abundant in juvenile ERBs
- Upon age progression, immune cells gain putative regulatory phenotypes

Authors

Virginia Friedrichs, Christophe Toussaint, Alexander Schäfer, ..., Anne Balkema-Buschmann, Antoine-Emmanuel Saliba, Anca Dorhoi

Correspondence

emmanuel.saliba@helmholtz-hiri.de (A.-E.S.),
anca.dorhoi@fli.de (A.D.)

In brief

Using a multipronged single-cell approach, Friedrichs et al. find that neutrophils, T cells, and CD206$^+$ myeloid cells are enriched in adult bats, whereas B cells and CD11b$^+$ T cells are more abundant in juveniles. Tissue dynamics and functions of immune cells in differentially aged ERBs grant insights into bat immunity.

Friedrichs et al., 2022, Cell Reports *40*, 111305
September 6, 2022
https://doi.org/10.1016/j.celrep.2022.111305

CellPress

Cell Reports

CellPress
OPEN ACCESS

Article

Landscape and age dynamics of immune cells in the Egyptian rousette bat

Virginia Friedrichs,[1,6,8] Christophe Toussaint,[2,8] Alexander Schäfer,[1] Melanie Rissmann,[3,7] Oliver Dietrich,[2] Thomas C. Mettenleiter,[4] Gang Pei,[1] Anne Balkema-Buschmann,[3] Antoine-Emmanuel Saliba,[2,*] and Anca Dorhoi[1,5,9,*]

[1]Institute of Immunology, Friedrich-Loeffler-Institut, Greifswald-Insel Riems, Germany
[2]Institute for RNA-based Infection Research (HIRI), Helmholtz Center for Infection Research (HZI), Würzburg, Germany
[3]Institute of Novel and Emerging Infectious Diseases, Friedrich-Loeffler-Institut, Greifswald-Insel Riems, Germany
[4]Friedrich-Loeffler-Institut, Greifswald-Insel Riems, Germany
[5]Faculty of Mathematics and Natural Sciences, University of Greifswald, Greifswald, Germany
[6]Present address: Institute of Diagnostic Virology, Friedrich-Loeffler-Institut, Greifswald-Insel Riems, Germany
[7]Present address: Erasmus University Medical Center, Rotterdam, Zuid Holland, the Netherlands
[8]These authors contributed equally
[9]Lead contact
*Correspondence: emmanuel.saliba@helmholtz-hiri.de (A.-E.S.), anca.dorhoi@fli.de (A.D.)
https://doi.org/10.1016/j.celrep.2022.111305

SUMMARY

Bats harbor high-impact zoonotic viruses often in the absence of disease manifestation. This restriction and disease tolerance possibly rely on specific immunological features. In-depth molecular characterization of cellular immunity and imprinting of age on leukocyte compartments remained unexplored in bats. We employ single-cell RNA sequencing (scRNA-seq) and establish immunostaining panels to characterize the immune cell landscape in juvenile, subadult, and adult Egyptian rousette bats (ERBs). Transcriptomic and flow cytometry data reveal conserved subsets and substantial enrichments of CD79a$^+$ B cells and CD11b$^+$ T cells in juvenile animals, whereas neutrophils, CD206$^+$ myeloid cells, and CD3$^+$ T cells dominate as bats reach adulthood. Despite differing frequencies, phagocytosis of circulating and tissue-resident myeloid cells and proliferation of peripheral and splenic lymphocytes are analogous in juvenile and adult ERBs. We provide a comprehensive map of the immune landscape in ERBs and show age-imprinted resilience progression and find that variability in cellular immunity only partly recapitulates mammalian archetypes.

INTRODUCTION

Despite belonging to one of the largest mammalian taxa, Chiroptera, with over 1,400 bat species described to date (Nowak and Walker, 1994), the bat immune system remained largely enigmatic until recently. An evolutionary paradigm of bats is their propensity to harbor the deadliest viruses known to man without displaying any clinical signs themselves. Zoonotic viruses originating from bats include rabies viruses, filoviruses such as Ebola virus (EBOV) and Marburg viruses (MARV), paramyxoviruses like Hendra virus (HeV) and Nipah virus (NiV), coronaviruses such as Middle East respiratory syndrome-related coronavirus (MERS-CoV), and presumably also severe acute respiratory syndrome coronavirus-2 (SARS-CoV-2). This variety indicates a long history of co-evolution between bats and their viruses (Baker et al., 2013), yet precise mechanisms underlying the propensity of bats to maintain and shed multiple viral pathogens remain to be elucidated. Several hypotheses have been postulated with respect to their reservoir potential, including flight-dependent regulation of anti-microbial immunity and reduced inflammation, leading to disease tolerance. The body temperature and metabolic rates of bats increase during flight (Kunz, 1982), which may enhance immune responses to facilitate defense against microbes. Regarding inflammatory responses, substantial differences in innate immunity have been reported. Bats detect and respond to RNA viruses, while DNA sensing is dampened, due to limited signaling via stimulator of interferon genes (STING) (Xie et al., 2018), absence of members of the pyrin and hematopoietic interferon-inducible nuclear (HIN) domain (PYHIN) (Zhang et al., 2013) gene family, and short pentraxins (Larson et al., 2021). Interestingly, interferon (IFN) expression is constitutive in steady state in several bat species (Bondet et al., 2021; Zhou et al., 2016b). Moreover, inflammation appears to be restricted, as shown by reduced activation of the NLR family pyrin domain containing 3 (NLRP3) inflammasome (Ahn et al., 2019) and limited bioactive interleukin (IL)-1β secretion (Ahn et al., 2019; Goh et al., 2020). Regardless of these immune traits, viral replication is inhibited efficiently (He et al., 2014; Pavlovich et al., 2018), and likely additional anti-viral features are peculiar to bats.

Studying bat immune systems has been severely hindered due to paucity of available tools (Wang et al., 2021). Most bat species are protected by law through federal nature conservation acts (Kingston et al., 2016), impeding sampling. Accordingly, *in vitro* data based on investigation in cell lines prevail (Banerjee

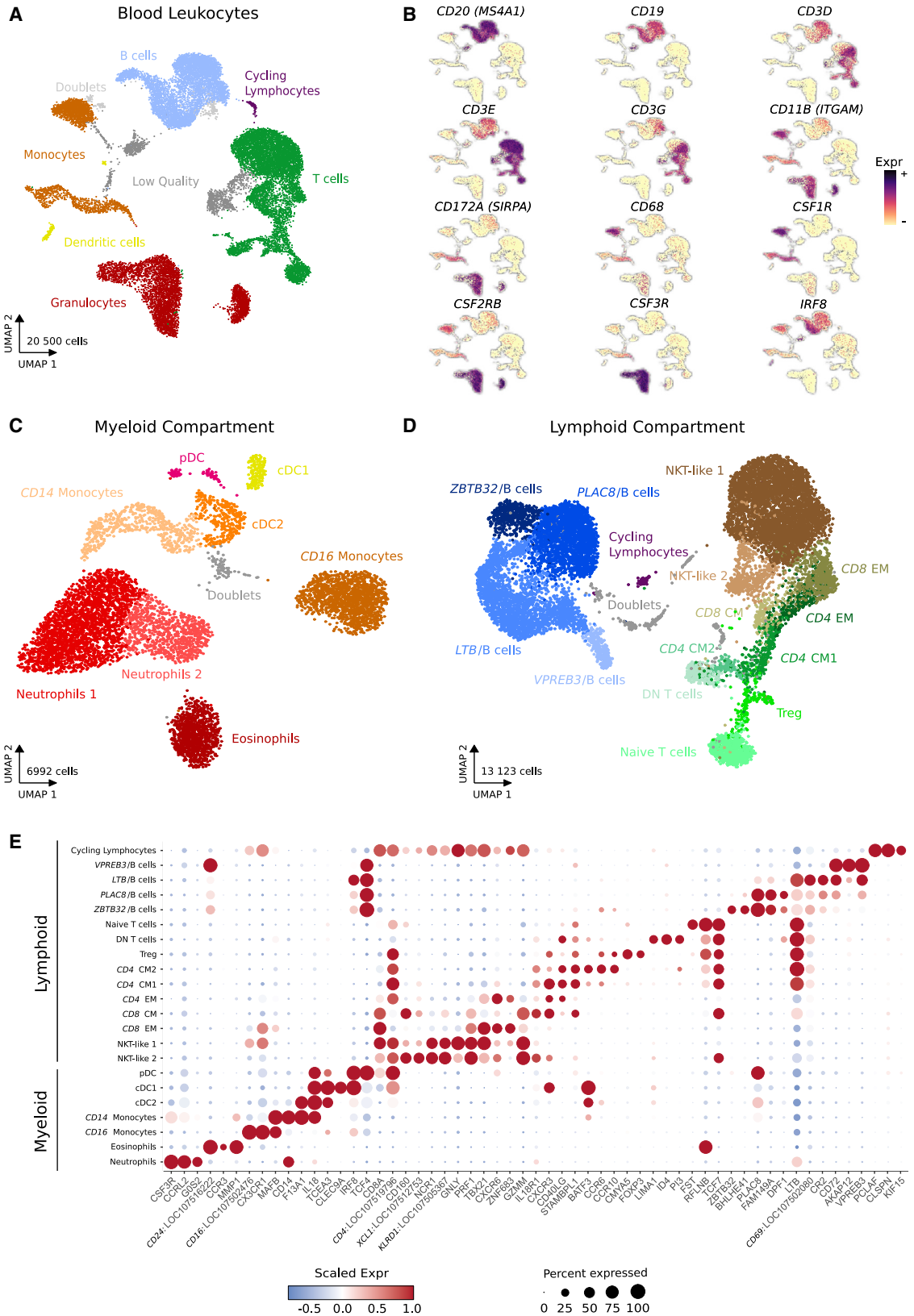

(legend on next page)

et al., 2020). Valuable *in vivo* insights have come from immune-targeted investigations in the pteropid bats *Eonycteris spelaea* and *Pteropus alecto*, both reservoirs for HeV (Edson et al., 2019), lyssaviruses (Moore et al., 2010), and betacoronaviruses (Vidgen et al., 2015). These bats have high frequencies of neutrophils (Becker et al., 2019; Martinez Gomez et al., 2016; Periasamy et al., 2019) and a majority of lymphocytes in blood, lymph nodes, and bone marrow consist of $CD4^+$ T cells, whereas $CD8^+$ T cells dominate in the spleen (Martinez Gomez et al., 2016). Moreover, T cells outnumber B cells in blood and spleen, and both subsets are activated and proliferate upon mitogenic stimulation in both species (Martinez Gomez et al., 2016). Details on cellular immune compartments in other bats are unknown. Considering the taxon richness, variations in size, diet, torpor habits, and global distribution (Kingston et al., 2016), focusing on a few species might bias knowledge of bat immunity and be misleading. This pertains to reservoir function because not every species supports maintenance and shedding of specific viruses equally (Guito et al., 2021; Halpin et al., 2011; Middleton et al., 2007; Williamson et al., 1998, 2000). The pteropid bat *Rousettus aegyptiacus* (Egyptian rousette bat [ERB]) is the main reservoir of MARV and susceptible to bat-specific influenza A viruses H9N2 and H18N11 (Kandeil et al., 2019). This species is used as an infection model for various agents, underlining the necessity to better understand its immune system. Immune cell subsets in ERB have not been defined yet. Appealing hypotheses regarding disease tolerance as a main mediator of ERB's reservoir ability await validation by comprehensive immunophenotyping approaches. Considering that tolerance restricts host-mediated pathology in human infants (Kollmann et al., 2017), effects of age on bat immunity also require careful consideration. Given their social behavior, notably mixing in large colonies, the distinct patterns of immunity in juvenile versus adult individuals may facilitate viral maintenance; i.e., inexperienced immunity enabling viral fitness.

Here, we implemented a multipronged approach to phenotype the transcriptome and epitopes of immune cells at the single-cell level of adult, subadult, and juvenile ERBs, and follow-up with functional characterization by monitoring phagocytic and proliferative capacity of defined cell types encompassing a total of 66 individuals (Figures S1A and S1B). Single-cell RNA sequencing (scRNA-seq) allowed us to delineate 22 transcriptomically different cell types and clusters of bat leukocytes, and flow cytometry confirmed the prevalence of B cells in juvenile animals, along with activated T cells. Myeloid cells with presumptive regulatory features were enriched in adult ERBs in both tissue and circulating blood. The diminished resilience patterns in juvenile animals diverge from observations recorded for human infants (Kollmann et al., 2017). Immunodevelopment (i.e., vulnerability of the developing individual due to undergoing immune maturation; Simon et al., 2015) and immunosenescence (Avery et al., 2014; i.e., weakened immune responses in older individuals) might adjust the spillover potential of adult and juvenile bats, as described for MARV (Amman et al., 2012).

RESULTS

Transcriptomic landscape of circulating immune cells in ERB blood

We performed scRNA-seq on freshly collected blood from four adults, two subadults, and three juveniles to explore the diversity of peripheral immune cells in ERB. Subsequent assays phenotypically and functionally characterized circulating and tissue-resident immune cells (Figure S1). Viability of sorted and red blood cell (RBC)-lysed leukocytes was assessed post sorting (Figures S2A and S2B) and indicated negligible cell death (around 5%–10%) and optimal cell recovery (above 95%) before scRNA-seq processing (Figures S2B and S2C). Cells from juvenile and adult individuals were pooled to minimize batch effects. Simultaneously, peripheral blood mononuclear cell (PBMC) samples of two subadult and one adult animals were prepared to investigate variations between whole-leukocyte and PBMC fractions. These were also pooled prior to single-cell partitioning. After sequencing and mapping to a recently published ERB genome (Jebb et al., 2020), we applied Souporcell (Heaton et al., 2020) to demultiplex the different individuals based on genetic variants and assign each single cell to a donor identity. Equal representation of each ERB individual was successfully achieved (Figure S2D).

Overall, we recovered 21,973 transcriptomes to select highly variable genes, performed dimensional reduction, and identified cell populations by unsupervised graph-based clustering (Figure 1A). Low-quality cells and doublets were easily discriminated by distinct clustering (Figures 1A and S2E) leaving 20,500 cells for downstream analysis. Using differentially expressed genes (DEGs), we assigned clusters to major immune cell types (Figures 1A and 1B), and myeloid and lymphoid lineages were further clustered separately to refine cell type annotation (Figures 1C and 1D). We based our cluster annotations on DEGs reported in the literature for human and mouse. Genes used for annotating cell identity proved conserved across mammals (Geirsdottir et al., 2019; La Manno et al., 2016; Papenfuss

Figure 1. scRNA-seq of circulating leukocytes in ERB blood

(A) Uniform Manifold Approximation and Projection (UMAP) representation of 21,973 cell transcriptomes from four adult, two subadult, and three juvenile ERBs, including whole-blood and PBMC samples; 20,500 single-cell transcriptomes were recovered after low-quality cell and doublet exclusion. Cell clusters (Leiden clustering) were grouped and colored according to major cell type classification based on main marker genes.

(B) Feature plots displaying log-normalized expression of main marker genes used to define the major cell types in (A).

(C) UMAP representation of the myeloid compartment after extracting transcriptomes from the granulocyte, monocyte, and dendritic cell groups identified in (A). A total of 6,992 single-cell transcriptomes was recovered after doublet exclusion.

(D) UMAP representation of the lymphoid compartment after extracting transcriptomes from the B cell, T cell, and cycling lymphocyte groups identified in (A). A total of 13,123 single-cell transcriptomes was recovered after doublet exclusion.

(E) Dot plot recapitulating a gene signature for each identified cell type in the myeloid and lymphoid compartments (C and D). Genes were selected among the top 25 DEGs sorted by the lowest p values for each cell cluster. Dot size is proportional to the percentage of cells with detectable expression of the indicated gene. Dot color is indicative of the average expression value for the indicated gene, scaled across all identified clusters.

et al., 2012). Overall, 22 different transcriptomic cell states could be delineated (Figures 1C–1E), which are available under the URL https://infection-atlas.org/Immubat-ERB-Blood/. B cell clusters exhibited a high expression of both canonical markers *CD20* (*MS4A1*) and *CD19*, whereas T cells specifically expressed the components of the TCR-CD3 complex *CD3D*, *CD3E*, and *CD3G* (Figures 1A and 1B). Remaining clusters constituted the myeloid compartment with expression of markers such as *ITGAM* (*CD11b*) or *SIRPA* (*CD172a*). Monocytes were identified as cells co-expressing *CD68* and *CSF1R*. Two different populations of granulocytes are present in ERB blood, marked by the strong expression of *CSF2RB* and *CSF3R*, respectively. Finally, the remaining myeloid clusters expressing *CD68* and notably the *IRF8* transcription factor were annotated as dendritic cells (DCs). The number of transcribed genes detected per transcriptome was highly related to the cell type and PBMC purification excluded granulocyte fractions, without affecting other leukocyte subsets (Figure S2F). Fewer than 1,000 genes were detected for granulocytes, in line with their expected low RNA content, while up to 5,000 genes were recovered from monocyte and DC subsets (Figure S2G). We examined DEGs to precisely annotate each of the 22 transcriptomic cell states (Table S1). Of note, the current ERB reference genome is incompletely annotated and many genes are only annotated with a LOC identifier (identifier for genes with no defined orthologs). When such genes were detected as differentially expressed, we performed BLAST (Blast Local Alignment Search Tool) searches to find similar sequences in the human genome and attribute them a human symbol name (Table S2). In case of moderate-to-low homology to human orthologs, we caution about assuming identical functions compared with their human orthologs without further validation.

We first refined the annotation of myeloid cells (Figures 1C, 1E, and S3A). The main granulocyte population is *CSF3R* positive and corresponds to neutrophils expressing *CCRL2*, *G0S2*, *PTGS2*, and *LTF*. The two granulocyte subclusters were correlated with the number of expressed genes detected per cell with no specific gene signature, reflecting variability or natural aging of the circulating neutrophil population under steady state rather than different cell states. The second granulocyte population lacks expression of *CSF3R* but presents a distinct gene expression signature, including matrix metalloproteinases (*MMP1* and *MMP9*), *GAPT*, and *OLIG1*. Other specific genes, such as *LTC4S*, *CCR3*, and *GATA1*, were highly suggestive of eosinophils or basophils. We finally annotated this cluster as eosinophils based on the expression of *CEBPE*, *CD24* (*LOC107516222*), and *PRG3* (*LOC107518414*). The granulocyte identity of neutrophil and eosinophil clusters is further confirmed by their depletion from PBMC fractions of corresponding samples (Figure S2F). Monocyte populations form two different clusters defined by the expression of either *CD14* or *CD16* (*LOC107502476*) (Figure S3A). *CD14* monocytes had the highest expression of *VCAN* and *MAFB*, whereas *CD16* monocytes expressed *CX3CR1* and *TNFRSF8*. DCs were readily classified as myeloid cDC1 (*CLEC9A*, *XCR1*) or plasmacytoid pDCs (*TCF4*, *CD8B*, *IRF7*). The increased resolution gained from focusing on the myeloid compartment led to the identification of an additional cluster merged with the *CD14*-expressing monocytes. Cells in this cluster do not express *CD14* or *CD16*, therefore challenging a monocytic identity. This cluster expressed *IL18*, *HMGN3*, and *TCEA3* and a transcriptomic profile close to cDC1. These observations, together with a high expression of various major histocompatibility complex class II (MHCII) components, are overall compatible with myeloid cDC2 (Dutertre et al., 2019). Considering that ERBs are natural reservoirs for filoviruses, we evaluated expression of host factors relevant for entry and replication of these pathogens in immune subsets. Multiple mononuclear myeloid subsets are enriched in factors endowing permissiveness for filoviruses, yet their levels differ for cDC versus monocytes (Figure S2H).

Second, we investigated in-depth the lymphoid compartment (Figures 1D, 1E, and S3B). We identified four B cell clusters, but were unable to link them to commonly reported human B cell subsets. A cell cluster highly expresses *VPREB3*, a protein likely involved in the assembly of the pre-B cell receptor, *AKAP12* and *CD72* (*VPREB3*/B cells). The second cluster was characterized by the highest expression levels of *LTB*, *IRF8*, *CD69* (*LOC107502080*), and *CR2* within the B cell compartment (*LTB*/B cells). The most abundant cluster is distinguished from the other B cell subsets by the upregulation of *PLAC8*, *FAM149A*, and *DPF1* (*PLAC8*/B cells). This cluster is also marked by an increased expression of *S100A4*, *S100A10*, and *S100A11* as well as *CD99* and *CD44*, two genes associated with B cell activation (Hathcock et al., 1993; Park et al., 1999). Cells from the last B cell cluster are very similar to the *PLAC8* high cluster but showed mainly specific expression of *ZBTB32* and *BHLHE41*, two transcription factors reported in activated/memory B cells (*ZBTB32*/B cells). Remaining lymphoid clusters were characterized by high expression of *CD3E*, *CD8A*, and *CD4* (*LOC107519796*) as expected for T cells. Although CD4 and CD8 T cells appear to segregate within most of T cell clusters, we did not find such separation for two clusters. Rather, expression data suggested that cells from these clusters are co-expressing both *CD4* and *CD8*. Notably, these populations exhibit markers specific to natural killer (NK) cells (*NCR1*, *FCER1G*, *KLRB1*, and *NKG2* as *LOC107516556* and *LOC107505617*; *KLRD1* as *LOC107505366* and *LOC107505367*) (Figure S3B). This combination of T cell and NK cell features prompted us to annotate these two clusters as NKT-like cells. These cells are also likely to exert a cytotoxic function (*PRF1*, *CTSW*, *GZMM*, and *GZMB* found as *LOC107513518* or *LOC107513519*). The more abundant cluster (NKT-like 1) expresses *GNLY* and shows increased *TBX21*, *CX3CR1*, and *GZMB* levels. The smaller NKT-like cluster (NKT-like 2) is characterized by the expression of *XCL1* (*LOC107512753*), *CD160* (an activating NK receptor), and *TCF7*. The remaining T cell population was refined based on *CD4* and *CD8* expression. We delineated a total of eight T cell clusters. The cluster of naive T cells is marked by the expression of *FST* and presents the highest expression of naive marker genes (*TCF7*, *LEF1*, *CCR7*) while being populated by both CD8 and CD4 T cells. The regulatory T cell (Treg) population exhibits a typical signature including the particular transcription factor *FOXP3*. We identified a T cell cluster with nearly no detectable expression of both *CD4* and *CD8* (Figure 1E), which we refer to hereafter as double-negative (DN) T cells. They exhibit an uncommon profile, but are marked by the expression of *PI3*, *ID4*, *LIMA1*, and the

macrophage colony-stimulating factor (*CSF1*). Human DN T cells have been reported with potential for immunosuppressive functions (Haug et al., 2019). We distinguished three supplementary clusters within the CD4 population. One cluster was marked by an increased expression of *GZMK*, *GZMB*, *TBX21*, *NKG7*, and *CXCR6* (involved in T cell maintenance at inflammation sites; Wein et al., 2019) as well as various activation markers (*CX3CR1*, *CCL5*, and *CCL4* as *LOC107503311*; *CCL3* as *LOC107506475*). We refer to this population as CD4 effector memory (CD4 EM). The two other CD4 clusters were identified as central memory cells based on the expression of *SELL* and *TCF7*. We distinguished two different subsets marked by the expression of *CD40LG* and *CXCR3* (CD4 CM1) or *BATF3* and *CCR10* (CD4 CM2). The CD8 population could be separated in two clusters corresponding to effector and central memory cells analogously to CD4 cells. The CD8 EM cluster presents a profile similar to CD4 EM but specifically expresses *PRF1* and *IL10*, while CD8 CM are characterized by the expression of *CD160*, *CD7*, and *CXCR3*. Finally, we found in the lymphoid compartment a cluster including a mixture of cycling lymphocytes with high expression of numerous genes related to cell cycle, such as *PCLAF*, *CLSPN*, or *KIF15*.

After characterizing the different cell clusters present in ERB blood, we investigated differences in abundancy of each annotated cell type upon maturation (Figures 2A and 2B). We performed a compositional analysis with scCODA, a tool tailored for single-cell analysis relying on a Bayesian approach to identify credible changes in cell type composition (Buttner et al., 2021). scCODA allows circumvention of the compositional biases inherent to single-cell experiments as the cell type counts reflect the proportion of each cell type in the sampled cell pool and are not representative of the absolute cell counts in ERB blood. We chose the cDC1 population for reference in the compositional analysis, as it is a cluster maximizing presence in all ERB individuals with minimal variation in abundancy. scCODA found four cell clusters compatible with differences between adult, subadult, and juvenile ERBs (Figures 2A and 2B). Neutrophils were more abundant in adults, whereas *PLAC8*$^+$ and *LTB*$^+$ B cell subsets were enriched in subadult and juvenile ERB (Figure 2B). *VPREB3*$^+$ B cells appeared to be less abundant in adults, but this discrepancy reached statistical significance only in comparison with juveniles. Therefore, B cells generally have a diminished presence among circulating leukocytes in adults.

Flow cytometry unveils variability in cell frequency and phenotype of the myeloid compartment

As scRNA-seq revealed that major lineage markers are conserved, we next aimed to establish flow cytometry panels enabling cost-effective ERB leukocyte phenotyping and cell type-specific sorting/isolation, which is a necessary prerequisite for various functional assays. Such assays can provide valuable information that are not recovered from scRNA-seq data alone. We screened 47 commercially available antibody clones (Table S3) and identified eight antibodies exhibiting cross-reactivity with bat leukocytes. These encompassed antibodies targeting surface (CD206, MHCII, CD11b, CD172a) and intracellular molecules (CD3, CD79a, Ki-67, T-bet [not shown]). Furthermore, amino acid sequences of antibodies that were cross-reactive to ERB leukocytes were aligned to human and mouse orthologs. While consensus ranged from 32.7% to 86.1%, identity between bat and human was slightly higher than bat to mouse (Table S4). We mapped the genes coding the cross-reactive molecules using the scRNA-seq cellular identities previously established (Figures 1B and 3A). An antibody targeting mouse and human cell adhesion molecule ITGAM (CD11b), which is a universal marker for myeloid cells and stains a subset of activated T cells (Christensen et al., 2001), cross-reacted with the ERB ortholog and was expressed in all myeloid clusters (Figures 1A and 3A). Further identification of myeloid cells was conducted utilizing antibodies targeting bovine signal regulatory protein α (SIRPα, CD172a) and human mannose receptor (CD206). The transcript of CD172a could be found in nearly all myeloid clusters, and CD206 is expressed by a small fraction within the monocyte cluster (Figures 1A and 3A). Based on the clusters expressing the respective transcripts, bat monocytes and DCs were defined in flow cytometry as CD11b$^+$CD172a$^+$ and an additional CD206$^+$ mononuclear myeloid cell (MMC) subset could be identified (Figure 3B). An antibody recognizing mouse MHCII only partly cross-reacted with bat MHCII (Figure S4A), presumably due to variability of the haplotypes in tested animals, and hence facilitated analyses when the staining was successful. For validation of antibody cross-reactivity, the following cell subsets were sorted and analyzed by microscopy: CD11b$^+$ CD172a$^-$, CD11b$^+$CD172a$^+$, CD172a$^-$, and FSC^{high}SSC^{high} cells. In addition, PCR was used to evaluate expression of several markers; i.e., CD3 (pan T cell), CD44, CD11b (pan myeloid), CD14 (monocyte), CD45 (*PTPRC*, pan leukocyte), CD68 (macrophage), CD79a (pan B cell), CD163 (monocyte/macrophage), and CD172a (monocyte/DC) in sorted cells (Figure S4B). CD11b$^+$CD172a$^+$ cells were spherical cells with an approximate nucleus to cytoplasm ratio of 3:1, indicating monocytic identity (Figure 3C), and this was further supported by gene transcript analysis; e.g., *SIRPA*, *CD163*, and *CD14* (Figure S4B). After extensive validation, we immunophenotyped mononuclear cells in ERB blood and found, in line with scRNA-seq observations, similar abundances of monocytes and DCs in both age groups (Figure 3D). However, frequencies of CD206$^+$ MMCs were significantly increased in adult bats and suggestive of enrichment of cells showing an M2-like phenotype and regulatory features in this group.

To gain deeper insights into immune cell abundances in various ERB tissues, we analyzed myeloid cells in blood, spleen, mesenteric lymph node (mLN), and lungs of adult and juvenile female bats (Figures 3E and 3F). CD11b$^+$CD172a$^+$ monocytes/macrophages and DCs (Figure 3E) were quantified in unperfused tissue. They were more abundant in lung compared with spleen and mLNs. CD206$^+$ myeloid cells, potentially macrophages, were predominantly found in the lung, and more in adult animals. Interestingly, both age groups displayed high and comparable frequencies of CD206$^+$ cells in the spleen.

To facilitate granulocyte identification in absence of cross-reactive antibodies, we used a gating strategy based on morphometric features of these cells. Granulocytes were defined as FSC^{high}SSC^{high} (subsequently detected to also be CD11b$^+$ CD172a$^+$) and positive for the viability stain, which originated from autofluorescence (Watt et al., 1980) (Figure 3G). FSC^{high}

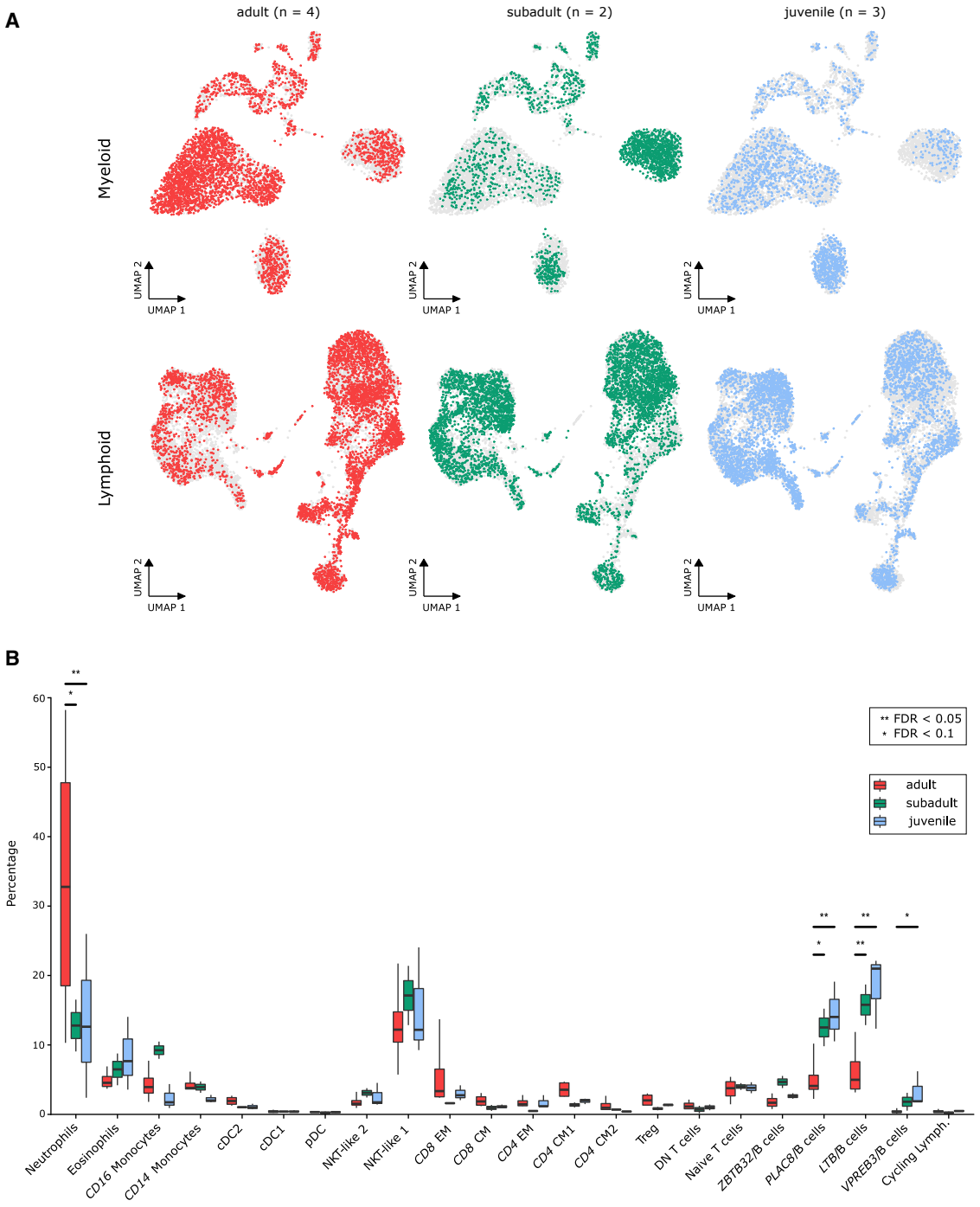

Figure 2. scRNA-seq-based compositional analysis of circulating leukocytes in adult and juvenile ERBs

(A) UMAP representations for both myeloid and lymphoid compartments. Cells are colored according to the age of donor bats (red, adults; green, subadults; blue, juveniles).

(B) Box plots of percentages of each identified cell type per age (four adults versus two subadults versus three juveniles). Significant differences detected by scCODA are indicated as stars (**FDR <0.05, *FDR < 0.1).

SSC^{high} cells showed a segmented nucleus and azurophilic granules, resembling neutrophils (Figure 3H). To confirm granulocyte identity, detection of neutrophil cytosolic factor expression by PCR (*NCF1*; Figure S4B) was used, as *CD66b* is absent in the latest ERB genome annotation, and no satisfactory primer pairs could be obtained for *CD56* or *CD15* detection. Detection of *CD16* (*LOC107502476*, mRouAeg1; Jebb et al., 2020; Figure S4B) rendered positive results for the fractions CD11b^{+}

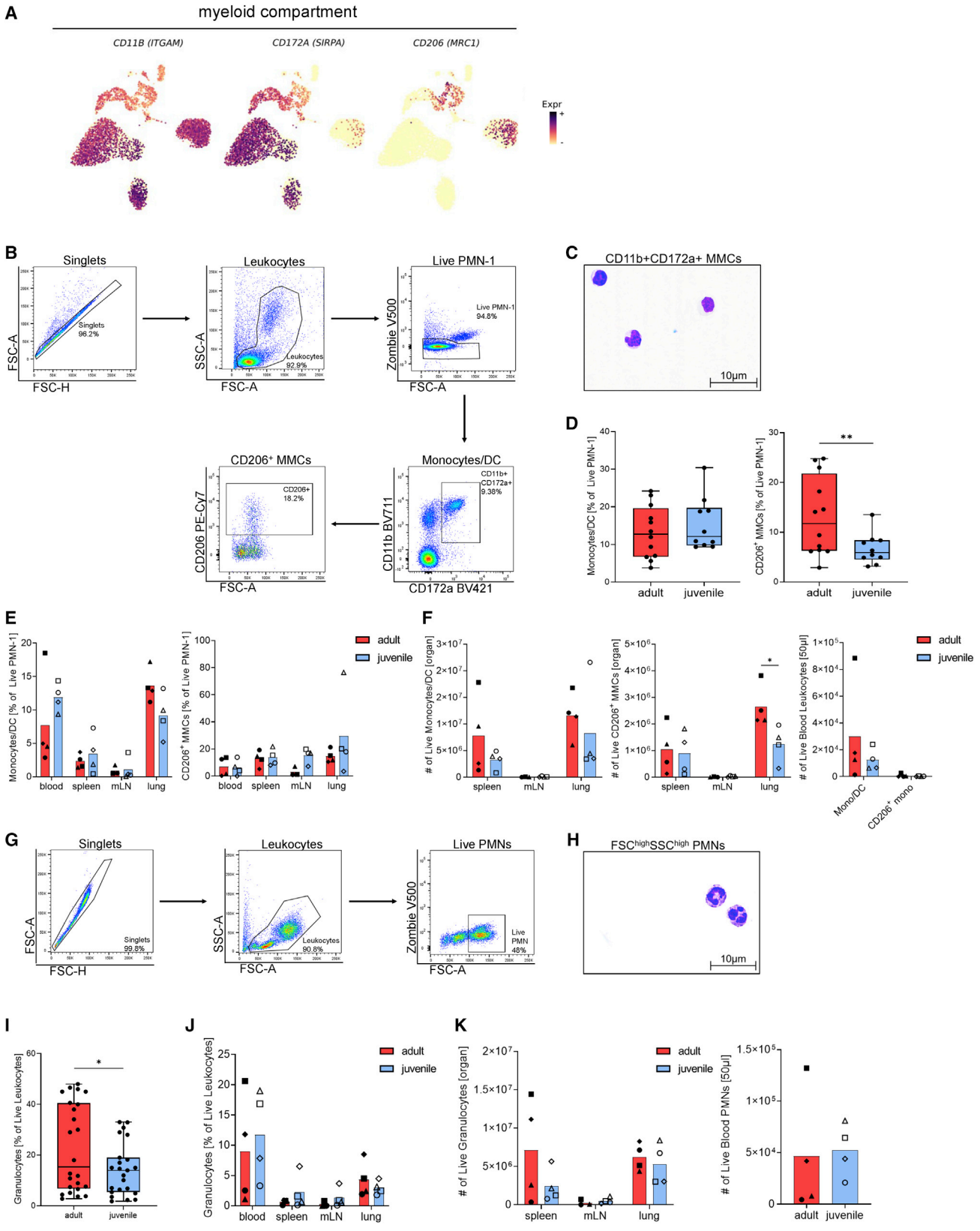

(legend on next page)

and CD11b^{+}CD172a^{+}, but not FSC^{high}SSC^{high}. In line with the transcriptomics data, frequencies of circulating granulocytes were significantly enriched in whole blood of adult bats (Figure 3I) but showed appreciable variation in the population we tested. Frequencies (Figure 3J) and numbers (Figure 3K) of granulocytes were high in spleen and lung and did not differ between the age groups. To validate granulocyte identity and also gain insights into subsets that are elusive in flow cytometry, blood smears of seven adult and nine juvenile ERBs were evaluated (Figures S5A and S5B). This analysis confirmed enrichment of neutrophils in adult bats and predominance of lymphocytes in juvenile ERBs (Figure S5A). Size and morphology of blood leukocytes did not differ between the age groups (Figure S5B).

Professional phagocytes largely maintain their activities with age in ERB

Phagocytic capacity of human granulocytes (Butcher et al., 2001; Simell et al., 2011; Wenisch et al., 2000) and monocytes/macrophages (Hearps et al., 2012; Plowden et al., 2004) declines with age. So far, studies in Yinpterochiroptera assessed phagocytic activity solely of bone marrow-derived macrophages but not primary phagocytes of differently aged individuals (Zhou et al., 2016a). We amended the gating strategy for myeloid cells to allow quantifying phagocytosis of *Escherichia coli* bioparticles (Figure 4A). In blood and lung samples, we observed increasing phagocytic rates over time for granulocytes (Figure 4B). Patterns of phagocytosis in monocytes and macrophages were similar to those detected in granulocytes (Figure 4C). For all populations evaluated, mean phagocytosis defined by geometric mean fluorescence intensity (gMFI) of internalized *E. coli* bioparticles did not differ significantly between the adult and juvenile groups (Figure S5C). Overall, abundances of blood phagocytes, which engulfed *E. coli* bioparticles, exceeded those recorded for lung samples, with the exception of the CD206^{+} subsets, which may represent alveolar macrophages (Figure 4D). A tendency for higher activity in adults compared with juveniles was observed irrespective of tissue and phagocyte population (except the CD206^{+} subset in blood), but failed to reach statistical significance.

Abundances of circulating T and B lymphocytes are age dependent in ERB

We further established a panel to identify T and B cells in ERB by flow cytometry. T cells were detected with an antibody targeting the cytoplasmic ε chain of the human T cell co-receptor CD3 with wide cross-reactivity to CD3 of mammalian species. Given the failure to detect the main T cell subsets (i.e., CD4 and CD8), we employed CD11b to identify putative activated T/effector cells, which express this integrin on subsets of activated CD8^{+} cells (Christensen et al., 2001; McFarland et al., 1992). We further screened antibodies recognizing antigens specific for B cells and identified an antibody targeting the cytoplasmic α chain of human B cell receptor (CD79a). As *CD3E* transcripts mapped to T cell clusters and *CD79A* transcripts to the B cell clusters, respectively (Figures 1B and 5A), T cells were identified using CD3 as a universal marker for T cells and CD79a as a pan B cell marker (Figure 5B). To confirm T and B cell identity, CD3^{+} and CD79a^{+} cells were sorted and validated for expression of lineage-specific cell markers via PCR (Figure S4B).

We observed significant differences in the abundance of circulating T and B cells in adult and juvenile bats. While frequencies of investigated leukocyte subsets (PMN, T, and B cells) did not differ between males and females (Figure S5D), adult ERBs displayed significantly higher frequencies of T cells compared with juvenile animals. Juvenile bats had more circulating B cells (Figure 5C). The results from adult ERBs are in line with data from *P. alecto* and *E. spelaea* (Gamage et al., 2020; Periasamy et al., 2019). As both specimens were caught from the wild and partly housed for at least 6 months prior to experiments (*E. spelaea*, Periasamy et al., 2019), the exact age of these bats was unknown. Presumably, *P. alecto* and *E. spelaea* bats already reached adulthood, since no thymus could be identified in these animals. In our study, the frequency of CD3^{+}CD11b^{+} T cells was significantly increased in juvenile bats (Figure 5C).

To gain a deeper insight into distribution of T and B cells in ERB tissues, we sampled various organs in addition to quantitative analysis of circulating lymphocytes; i.e. spleen, mLN, and lung in adult and juvenile animals (Figures 5D and 5E). Frequencies and absolute cell counts concurred for peripheral lymphocytes. Significant differences in frequencies were confirmed for both T and B cells. Total cell numbers further substantiated these findings for both circulating subsets. In the spleen, the patterns of T and B cell distribution matched those detected in peripheral blood. Adult ERBs displayed a similar frequency but higher total cell number of T cells in the spleen than juveniles. For

Figure 3. Identification of ERB myeloid cells in blood and organs by flow cytometry

(A) Gene expression of *ITGAM*, *SIRPA*, and *MRC1* across myeloid cells color coded and projected on the UMAP representation of scRNA-seq as detailed in Figure 1.

(B) Gating strategy for identification of monocytes/DCs and CD206^{+} mononuclear myeloid cells (MMCs). Live mononuclear cells (MNCs) (Zombie^{-} cells, granulocytes [PMNs] $^{-}$) were defined as monocytes/DCs (CD11b^{+}CD172a^{+}) and a CD206^{+} MMC subset was additionally evaluated.

(C) Cytomorphology of sorted CD11b^{+}CD172a^{+} MNCs.

(D) Frequencies of monocytes/DCs (CD11b^{+}CD172a^{+}) and CD206^{+} MMCs in the blood (adult, n = 12; juvenile, n = 10).

(E and F) (E) Frequencies and (F) numbers of monocytes/DCs (CD11b^{+}CD172a^{+}) and CD206^{+} MMCs from blood, spleen, mesenteric lymph node (mLN), and lung (n = 4/group).

(G) Gating strategy to identify ERB PMNs.

(H) Cytomorphology of sorted FSC^{high}SSC^{high} PMNs.

(I) Frequencies of circulating PMNs (adults, n = 23; juvenile, n = 21).

(J) Frequencies of PMNs in blood, spleen, mLN, and lung (n = 4/group).

(K) Numbers of PMNs in spleen, mLN, lung, and blood. Individuals are represented by dots, median ± interquartile range (IQR) (D and I) or each individual is represented by a specific symbol, bars depict group mean (E, F, J, and K). *$p < 0.05$, **$p < 0.01$, defined by unpaired t test.

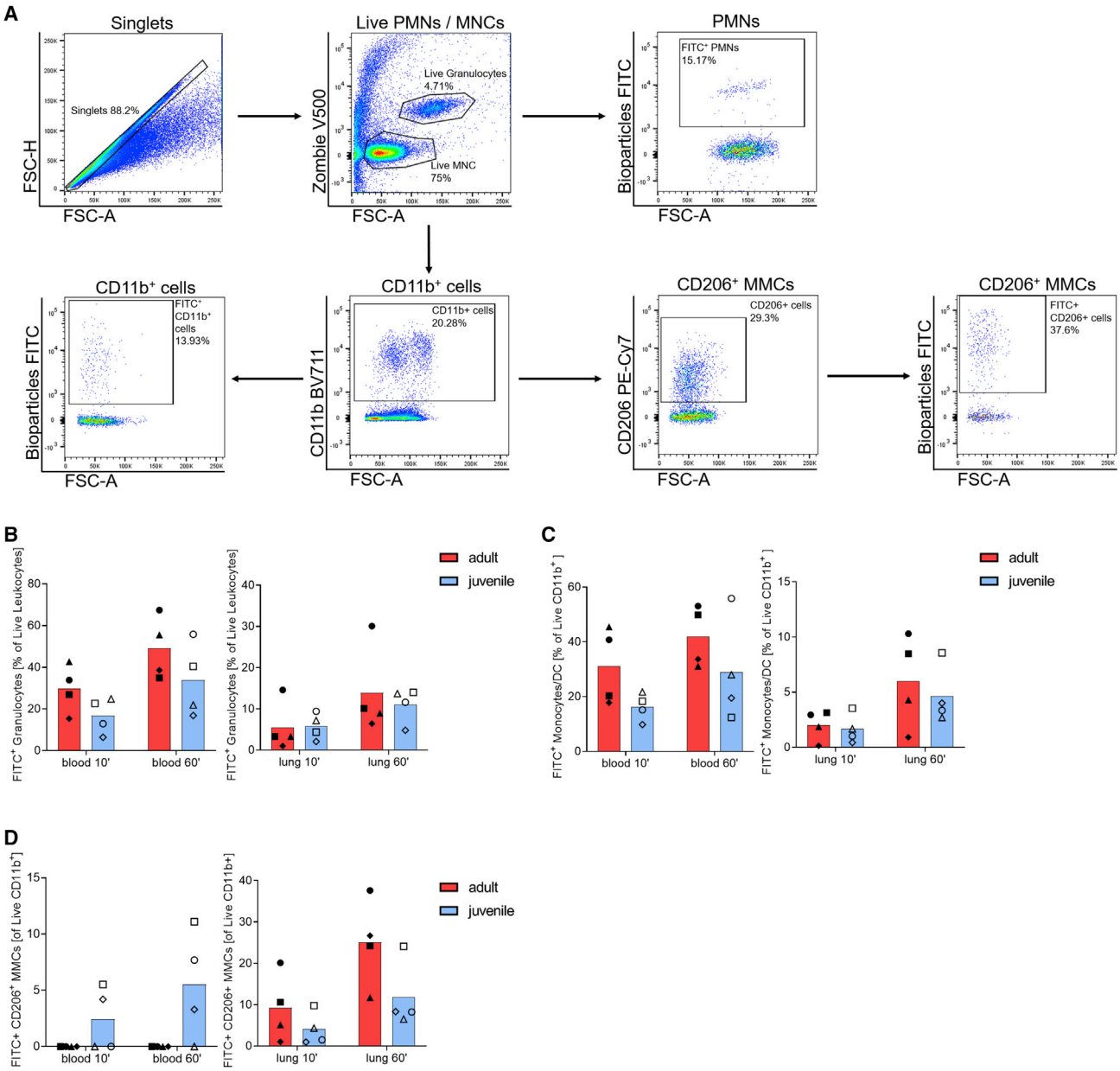

Figure 4. Functional characterization of ERB phagocytes

(A) Gating strategy to identify myeloid cells phagocytosing fluorescein-labeled *E. coli* bioparticles. Fluorescein isothiocyanate-positive (FITC$^+$) monocytes/DCs (CD11b$^+$PMN-1), CD206$^+$ MMCs, and granulocytes (PMNs) were analyzed.

(B–D) Frequencies of PMNs (B), monocytes/DCs (C), and CD206$^+$ MMCs (D) that internalized *E. coli* bioparticles (n = 4/group). Each individual is represented by a specific symbol, bars depict group mean.

splenocytes, matching observations from blood samples, the pattern for B cells was the opposite. In lymph nodes, a tendency for enrichment of B cells in juvenile animals was noticed, whereas abundances of B cells in the lung were comparable in the different age groups. Tissue specificities relative to variability in lymphocyte subsets (i.e., observable in blood and spleen, but not in lung) is of note in ERBs of variable age. Both frequency and absolute numbers of activated T cells (CD11b$^+$) were significantly higher in the lungs of juvenile ERBs (Figure 5D), whereas this subset was significantly higher in blood of juveniles in evaluation of absolute numbers (Figure 5E). Thus, progression to adulthood changes T/B cell ratio and possibly limits expansion of activated T cells.

Lymphocyte proliferation capacity is unchanged with age

Previous studies performed in *P. alecto* and *E. spelaea* indicated that lymphocyte-driven immune responses in bats are more

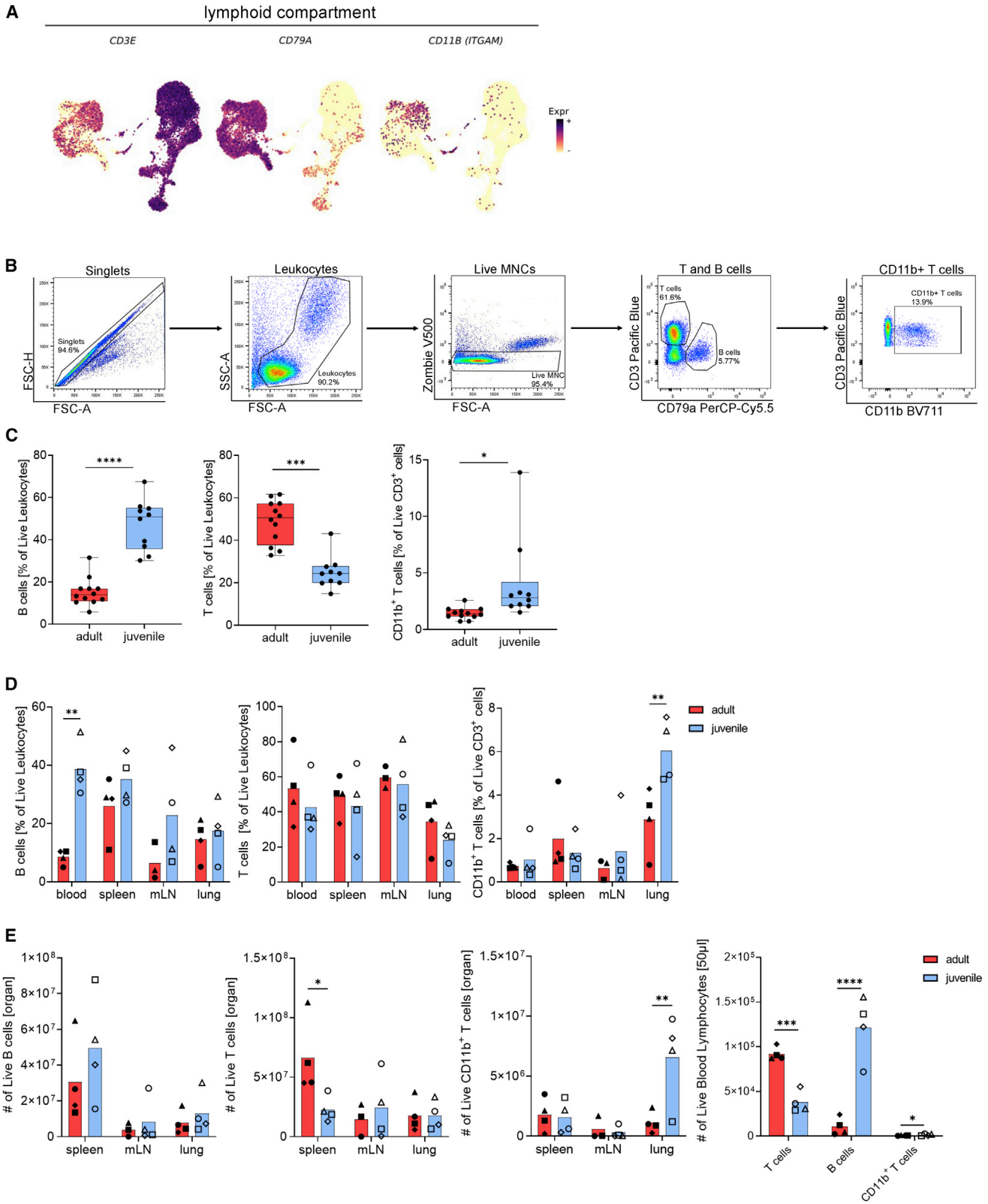

(legend on next page)

similar to those in humans than in mice (Martinez Gomez et al., 2016). To clarify the proliferative potential of ERB lymphocytes, PBMCs and splenocytes of adult and juvenile bats were stimulated *ex vivo* with either concanavalin A (ConA), lipopolysaccharide (LPS), or staphylococcal enterotoxin B (SEB) to specifically induce T and/or B cell proliferation. Proliferation was assessed using an amended version of the gating strategy of bat lymphocytes (Figures 5B and 6A). T cells proliferated upon ConA and SEB stimulation, and B cells expanded after LPS and SEB treatment (Figures 6B and 6C), as evaluated by Ki-67 staining. Ki-67-defined proliferation rendered overall more accurate results for splenocytes than PBMCs. Mitogenic stimulation resulted in a significant proliferation of splenic T cells irrespective of age (Figure 6B). Significant B cell proliferation was detectable in both groups (Figure 6C). Generally, the proliferative capacity of peripheral T and B cells was lower compared with splenic T and B cells in both adult and juvenile bats (Figures 6B, 6C, and S6). As internal control, we included the fluorescent cell staining dye carboxyfluorescein succinimidyl ester (CFSE) to detect proliferation (Figure S6). Interestingly, splenic and peripheral B cells responded to SEB, in addition to LPS, although to a lesser extent than T cells. Notably, analysis of $CFSE^{low}$ cells delivered more precise results for PBMCs over splenocytes. Significant proliferation in peripheral T cells of both adult and juvenile ERBs was observed upon mitogenic stimulation (Figure S6). These findings demonstrate the value of using concurrent CFSE and Ki-67 staining to accurately assess the proliferative activity of bat lymphocytes and highlight that mitogen-induced proliferation is uncoupled from age in ERB.

DISCUSSION

Deciphering host-pathogen interactions in natural reservoirs is critical for the understanding and containment of emerging zoonotic diseases, highlighting the importance of studies of bat immunity (Wang et al., 2021). Using a combined approach, we delineated seven myeloid and 15 lymphoid subsets with scRNA-seq and further characterized by flow cytometry seven immune cell populations, including T and B cells, monocytes, macrophages, granulocytes, and DCs in blood and organs of adult and juvenile ERBs. Our study unveils substantial differences in abundances and phenotypes of major immune cell types in relation to age in ERBs. These findings indicate that disease tolerance may establish upon reaching adulthood and could modulate pathogen dynamics in individual animals and possibly pathogen spread.

Studies on the morphology of bat lymphocytes date back to the late 1980s, describing lymphocyte-like cells in *Pteropus giganteus* (Chakravarty and Paul, 1987). More recent investigations focusing on *P. alecto* lymphocytes provided the first evidence for a delayed response upon mitogenic stimulation compared with mice (Chakravarty and Sarkar, 1994; Martinez Gomez et al., 2016; Sarkar and Chakravarty, 1991). We employed various mitogens and proliferation assays and observed that T and B cell proliferative responses are largely similar in adult and juvenile ERB, and comparable with adult individuals of other bat species (Martinez Gomez et al., 2016). Interestingly, splenic B cells consistently reacted to mitogenic stimulation only in juvenile bats, which indicates the presence of tissue-specific reactogenic B cells in association with an incomplete immune maturation process (Piatosa et al., 2010). Similar observations are frequently reported in other species, i.e. humans, especially in the context of vaccination and administration of common adjuvants (Burny et al., 2017). This finding may explain poor antibody responses upon experimental infection of ERB with EBOV/MARV (Guito et al., 2021; Paweska et al., 2016) and development of higher titers in very young ERBs after MARV challenge (Storm et al., 2018). These findings suggest that bats evolved toward tolerating viral replication, as confirmed by high viral loads in EBOV/MARV-infected ERBs, rather than viral clearance; e.g., by humoral immunity. Recent studies have provided essential insights into cross-reactivities of commercially available antibodies to *P. alecto* and *E. spelaea* immune cells, as well as in-depth phenotypic and functional characterization of major leukocyte populations in both species (Martinez Gomez et al., 2016; Periasamy et al., 2019). We found limited cross-reactivity with immune cell epitopes of ERBs. Bats are the second largest mammalian taxon with global distribution. Thus, immunological differences among species are to be expected given species-specific physiology possibly shaped by microbiomes and habitats. In addition, most studies rely on samples derived from wild-caught individuals (Gamage et al., 2020; Martinez Gomez et al., 2016; Periasamy et al., 2019). This inevitably leads to higher variances and obstacles in data interpretation, affecting reproducibility due to differing immune statuses and unknown age of wild-caught individuals (Periasamy et al., 2019). Since age shapes frequencies and subset distribution of leukocytes, as we found for ERBs, it must be carefully considered when analyzing immune parameters in wild bats. We profiled ERB immune cells from a captive colony maintained under constant climatic conditions and a supervised health status. ERB-specific age variations may be modulated by environmental and physiological factors, including stress. This is of particular interest, as clean housing alters immune cell development, as demonstrated for neutrophils in mice (Ince et al., 2018; Keresztes et al., 2007). Extension of our findings to wild-living ERBs is now feasible based on herein-reported profiling strategies. Our findings describe fundamental variations in immune cell profiles of adult and juvenile ERB blood and selected tissues; however, evaluation of additional organs should be considered in future studies.

Figure 5. Identification of ERB lymphocytes in blood and organs by flow cytometry

(A) Gene expression of *CD3E*, *CD79A*, and *ITGAM* across lymphoid cells color coded and projected on the UMAP representation of scRNA-seq as detailed in Figure 1.

(B) Gating strategy to identify bat T ($CD3^+CD79a^-$) and B ($CD3^-CD79a^+$) cells, and an activated T cell subset ($CD3^+CD79a^-CD11b^+$).

(C) Frequencies of lymphocytes in blood (adult, n = 12; juvenile, n = 10).

(D and E) (D) Frequencies and (E) numbers of lymphocytes in blood, spleen, mLN, and lung (n = 4/group). Individuals are represented by dots, median ± IQR (C) or each individual is represented by a specific symbol, bars depict group mean (D and E). *p < 0.05, **p < 0.01, ***p < 0.001, ****p < 0.0001, defined by unpaired t test.

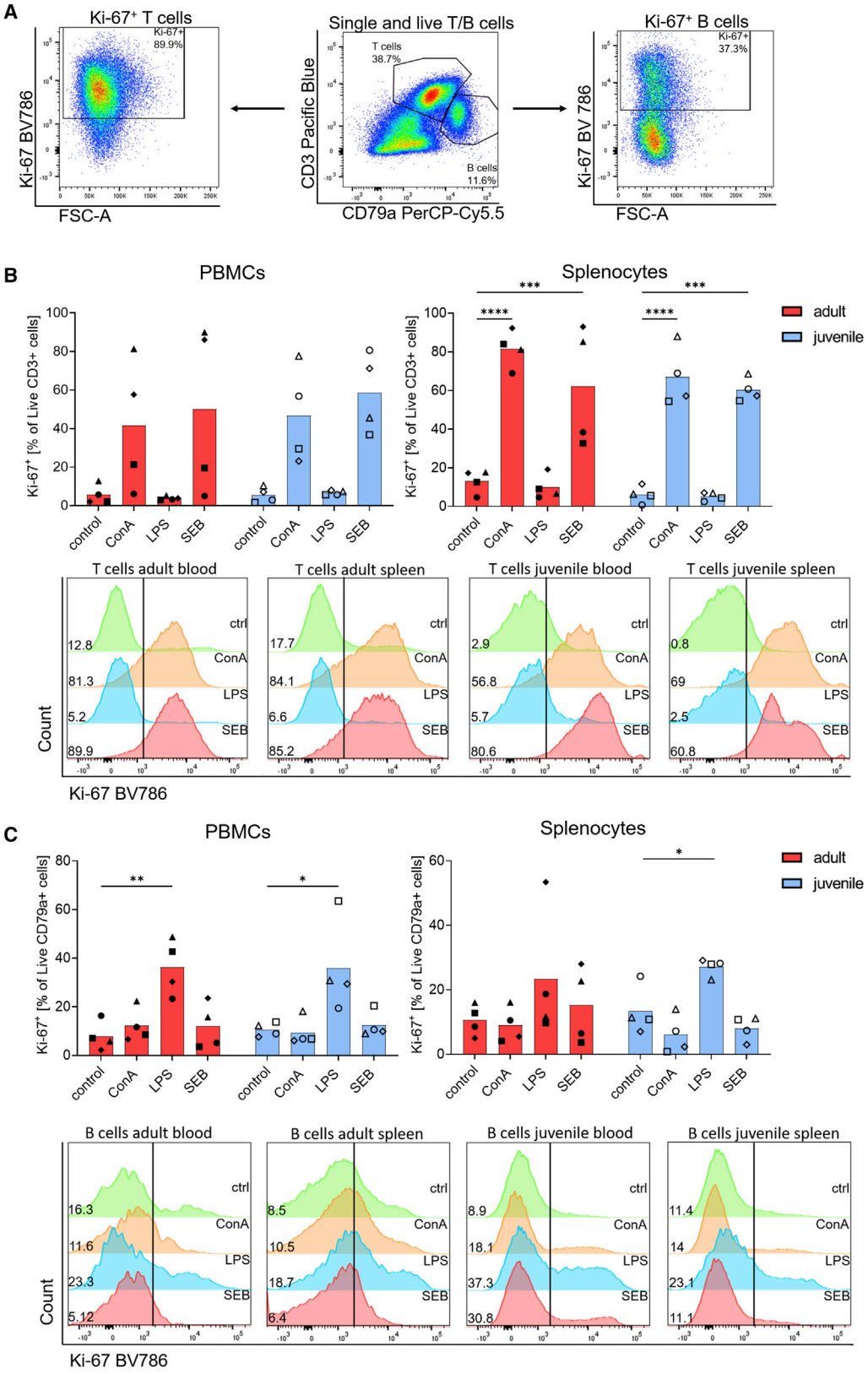

(legend on next page)

Current investigations of bat immunity at genomic and transcriptional level led to striking findings like constitutive IFN expression and dampened DNA sensing in some bats (Ahn et al., 2016, 2019; Xie et al., 2018), yet knowledge about bat immune cell phenotypes and functions is scarce. Whole-genome sequences and transcriptomes of different bat species enabled *in silico* analyses of the bat immune system (Jebb et al., 2020; Lee et al., 2015; Papenfuss et al., 2012; Pavlovich et al., 2018). Whole-genome sequencing (WGS) data revealed that the overall phenotype of bat immune cells resembles the one known from human and mice. However, only high-resolution methods like scRNA-seq could successfully unveil elusive leukocyte subsets; e.g. 2 NKT-like subsets in the periphery of adult and juvenile ERBs. The captured transcripts facilitate generation of monoclonal antibodies for accurate leukocyte identification in ERBs, as ERB-specific monoclonal antibodies for CD14 and CD19 could already be generated successfully elsewhere (Guito et al., 2021). Furthermore, building the landscape of circulating immune cells in ERBs advances the current understanding about cellular immunity in bats. The strategy for cluster annotation assumes that marker genes are correctly annotated and execute functions comparable with their human orthologs. Similar approaches have been applied to mammalian species other than mice and humans, i.e., domestic pigs (Herrera-Uribe et al., 2021) and horses (Patel et al., 2021), or wildlife species such as the naked mole-rat (Hilton et al., 2019). Moreover, human immune genes are phylogenetically closer to bat than to rodent orthologs (Gamage et al., 2020). We enriched the annotation of the reference ERB genome with BLAST searches of the top DEGs. While these genes provided support to annotate clusters, we were cautious about assuming identical functions compared with their human orthologs without further validation, particularly when we found a moderate or low homology (Table S2). The incomplete annotation of the current ERB genome requires consideration for annotation processes. Specific immune cell markers (e.g., CD16) lack proper annotation and can only be detected by mapping the LOC sequence to CD16 sequences in other species.

Our single-cell dataset complements previous studies conducted on PBMCs with flow cytometry. Overall, we found similar proportions of leukocyte populations to *E. spelaea* (Gamage et al., 2020). A subset of circulating monocytes was reported to express CD206 and MHCII, matching the cDC2 population we identified in ERB via scRNA-seq. The major population of circulating T cells in *P. alecto* lacks *TBX21* (T-bet), *EOMES*, and *GATA3* (Martinez Gomez et al., 2016). Considering our RNA expression data, this population possibly corresponds to naive T cells. Interestingly, we found that NKT-like cells co-expressing *TBX21* and *EOMES* are the dominating T cell subtype in ERB. We note a balanced representation of *CD4*- and *CD8*-expressing T cells in ERB, while $CD4^+$ T cells are nearly absent in *Rhinolophus sinicus* (Ren et al., 2020). In *P. alecto* $CD4^+$ T cells are predominant. Variations in leukocyte abundances across bat species should be validated by comparative evaluation of RNA and protein expression profiles. Thus, findings in specific species should be cautiously extended to other bats. Strikingly, adult ERBs showed high T cell abundances, while juveniles had higher frequencies and absolute numbers of B cells in all tested tissues. These age-related lymphocyte frequency patterns have been reported for humans (Piatosa et al., 2010; Valiathan et al., 2016). However, the differences between frequencies and absolute numbers are more distinctive in bats and could possibly affect their roles as reservoirs for human pathogens. Furthermore, juvenile bats exhibited higher frequencies and absolute numbers of $CD11b^+$ T cells, presumably activated $CD8^+$ T cells (McFarland et al., 1992), indicating an immune maturation process the adult specimens already completed (Christensen et al., 2001). Although we identified four B cell clusters, annotating them precisely remained challenging. Gene patterns presented in a recent study of peripheral human B cells suggest that *VPREB3*, *LTB*, and *PLAC8* clusters could correspond to transitional, naïve, and activated B cells, respectively (Stewart et al., 2021). B cell phenotypes can be partially discriminated through the detection of IgH class switching. However, the IGH locus is not annotated in the current ERB reference genome, thus hampering the annotation of B cell subsets with confidence. Future studies could refine ERB B cell identities, as the IGH locus is further characterized (Larson et al., 2021) and adequate tools to determine immunoglobulin secretion and function are established. Besides the general enrichment in B cells for juveniles, we found a particular interest for the *VPREB3*-expressing B cell cluster as it seems to be almost absent in adult specimens.

The granulocyte frequencies we observed in the periphery of both adult and juvenile ERBs drastically differ from those reported in *P. alecto* (Periasamy et al., 2019). This might be explained by species-specific differences. Moreover, ERBs at our institute are housed in quarantine conditions, whereas *P. alecto* specimens were wild-caught and then subjected to experiments (Periasamy et al., 2019). Hygiene and housing of animals greatly influence the number of circulating granulocytes, as reported for mice (Abolins et al., 2017). The frequencies we recorded might not reflect the proportion of circulating granulocytes in wild ERBs and this should be validated in future comparative studies. Previous reports described contradictory findings with significantly higher leukocyte counts in captive ERBs. However, animals reported as captive in the study were wild-caught and housed for several weeks, which most likely resulted in leukocytosis due to stress (Van Der Westhuyzen, 1988). Of note, especially for adult ERBs included in this study, a great variance in frequencies of circulating granulocytes was obvious, indicating that environmental factors related to breeding and maintenance, e.g., sampling-related stress, could greatly alter the frequency of circulating granulocytes, as reported for humans and mice (Ince et al., 2018; Keresztes et al., 2007).

Figure 6. Assessment of proliferative capacity of ERB lymphocytes upon mitogenic stimulation

(A) Gating strategy to identify $Ki\text{-}67^+$ proliferating lymphocytes.

(B and C) Proliferative activity of $CD3^+$ T cells (B) and $CD79a^+$ B cells (C) upon stimulation with ConA, LPS, or SEB was assessed for PBMCs and splenocytes (n = 4/group). Each individual is represented by a specific symbol, bars depict group mean, and histograms show representative mean fluorescence intensities for adult and juvenile bats. *$p < 0.05$, **$p < 0.01$,***$p < 0.001$, ****$p < 0.0001$ defined by paired t test.

Additionally, the significantly higher abundance of circulating granulocytes in adult compared with juvenile ERBs could reflect an increase with maturation, as already described for human infants and elderly (Valiathan et al., 2016). The phagocytic activity of bat granulocytes was slightly lower compared with that described in mice and humans (Gupta-Wright et al., 2017). Whether this relies on species-specific differences or the impairing effect of isoflurane-based sedation during blood withdrawal on cellular activity (Markovic et al., 1993) remains to be validated. Overall, ERB granulocytes can successfully be assigned utilizing the gating strategy defined here, and future studies should address potential differences in reactivity between adult and juvenile ERB neutrophils. Thus, evaluation of microbial killing in comparative approaches is mandatory to further elucidate the impact of age on functional variability.

Overall, the age-related findings are of relevance, because MARV infections reported in several African countries (Bausch et al., 2006; Timen et al., 2009)[,] were found to correlate with ERB birthing periods (Amman et al., 2012; Towner et al., 2007, 2009). Levels of active MARV infection range from 15% in 6-month-old juveniles to 2% in adults. These differences in active viral infection observed in juvenile and adult bats reinforce the hypothesis of bats prioritizing immune resilience over excessive inflammation upon maturation (Irving et al., 2021). This is supported by reports of naturally and experimentally infected bats displaying no clinical signs of disease upon infection with EBOV, bat coronavirus, MERS-CoV, and NiV, while mounting a humoral immune response and exhibiting high viral loads (Middleton et al., 2007; Munster et al., 2016; Swanepoel et al., 2007; Watanabe et al., 2010). These studies indicate that the immune system of bats evolved toward tolerating viral infection rather than actively reducing it, which might not be feasible due to high metabolic demands during flight. Age may be critical in balancing energy demands for growth and host defense versus physiologic behavior in bats and thus tailor cellular effectors to specific response patterns, notably disease resistance versus disease tolerance. Evidence for disease tolerance comes from findings related to humoral immunity in ERB (Larson et al., 2021). Our findings further substantiate the tolerance hypothesis by establishing proof that it is potentially linked to immunodevelopment in bats and embedded in cellular components as well, as indicated by a higher abundance of putative regulatory $CD206^{+}$ myeloid cells in adults and putative activated $CD11b^{+}$ T cells and *PLAC8* expressing B cells in juveniles.

Our study provides fundamental insights into the immunological fingerprint of ERB upon maturation, a natural reservoir for zoonotic viruses. The age imprinting on immune features highlights that immune maturation and resilience could modulate spillover events and must be considered in investigations focusing on host-pathogen interplay in ERB, and more generally in other *Chiroptera* species.

Limitations of the study

While scRNA-seq unveiled blood cellular cluster composition, subset definition remained limited by the use of lineage markers previously known from humans and mice, which could impair identification of possible ERB-specific markers and subsets. Along this line, our study is restricted by the paucity of ERB-specific or cross-reactive antibodies, hampering in-depth and comprehensive functional characterization of cell subsets identified by scRNA-seq. Validation of the findings in other bat species is required in order to put the age dependency into a broader chiropteran context. Our study assessed immune populations in selected ERB organs, but does not provide an immune cell atlas for all tissues. It is limited with respect to the sample size, particularly for analyses focusing on tissue profiling. Increasing the number of individuals is of particular importance, also because captive bat colonies may not recapitulate the genetic heterogeneity and microbial experience of wild-living animals. Analysis of wild ERBs could in addition provide essential insight into aged animals; i.e., above 10 years old. Due to breeding and colony management, the individuals kept at research colonies do not reach the average life expectancy of ca. 25 years of captive ERBs. Sampling wild-living bats thus would be essential to extend the findings to genetically diverse ERBs as well as to cover a broader age spectrum.

STAR★METHODS

Detailed methods are provided in the online version of this paper and include the following:

- KEY RESOURCES TABLE
- RESOURCE AVAILABILITY
  - Lead contact
  - Materials availability
  - Data and code availability
- EXPERIMENTAL MODEL AND SUBJECT DETAILS
  - Animals and animal housing
- METHOD DETAILS
  - Blood and tissue sampling
  - Tissue preparation
  - Processing of blood cells for scRNA-seq
  - Chromium GEM and library generation for scRNA-seq
  - Sequencing of scRNA-seq libraries, data pre-processing and custom cellranger genome generation
  - In silico analysis
  - Validation of antibody specificity
  - Blood smears
  - Flow cytometry
  - Phagocytosis assay
  - Mitogenic cell stimulation
- QUANTIFICATION AND STATISTICAL ANALYSIS
  - Analysis of scRNA-seq data
  - Analysis of flow cytometry data

SUPPLEMENTAL INFORMATION

Supplemental information can be found online at https://doi.org/10.1016/j.celrep.2022.111305.

ACKNOWLEDGMENTS

This study was funded by intramural funds from the Friedrich-Loeffler-Institut and was financially supported by Initialisierung- und Vernetzungsfonds für Infektionsforschung Greifswald, an initiative of Friedrich-Loeffler-Institut,

Helmholtz Center for Infection Research and University of Greifswald, Project Immubat. A.E.S. and C.T. thank Bundesministerium für Bildung und Forschung (BMBF) for support via the grant HOPARL (#031L0289B). We thank Marcel Bokelmann for assistance with blood sample collection as well as Silke Rehbein and Lisa Loerzer for excellent technical assistance and all animal caretakers for maintaining ideal standards for the bat colony. We further thank Alexander Leipold for supporting data analysis.

AUTHOR CONTRIBUTIONS

V.F. and A.S. performed experiments. A.B.B. and M.R. provided blood samples. A.B.B., M.R., A.S., and V.F. performed necropsies. C.T. and A.E.S. performed sequencing and annotation of scRNA-seq data. V.F., A.S., and C.T. analyzed data. O.D. provided scRNA-seq analytical tools. G.P., A.E.S., and A.D. provided assistance. G.P., A.E.S., and A.D. supervised the study. T.C.M., A.E.S., and A.D. acquired funding. A.D. designed the study. V.F., C.T., A.E.S., and A.D. wrote the manuscript. All authors reviewed the manuscript.

DECLARATION OF INTERESTS

The authors declare no competing interests.

Received: December 7, 2021
Revised: May 20, 2022
Accepted: August 10, 2022
Published: September 6, 2022

REFERENCES

Abolins, S., King, E.C., Lazarou, L., Weldon, L., Hughes, L., Drescher, P., Raynes, J.G., Hafalla, J.C.R., Viney, M.E., and Riley, E.M. (2017). The comparative immunology of wild and laboratory mice, *Mus musculus domesticus*. Nat. Commun. *8*, 14811. https://doi.org/10.1038/ncomms14811.

Ahn, M., Anderson, D.E., Zhang, Q., Tan, C.W., Lim, B.L., Luko, K., Wen, M., Chia, W.N., Mani, S., Wang, L.C., et al. (2019). Dampened NLRP3-mediated inflammation in bats and implications for a special viral reservoir host. Nat. Microbiol. *4*, 789–799. https://doi.org/10.1038/s41564-019-0371-3.

Ahn, M., Cui, J., Irving, A.T., and Wang, L.F. (2016). Unique loss of the PYHIN gene family in bats amongst mammals: implications for inflammasome sensing. Sci. Rep. *6*, 21722. https://doi.org/10.1038/srep21722.

Amman, B.R., Carroll, S.A., Reed, Z.D., Sealy, T.K., Balinandi, S., Swanepoel, R., Kemp, A., Erickson, B.R., Comer, J.A., Campbell, S., et al. (2012). Seasonal pulses of Marburg virus circulation in juvenile *Rousettus aegyptiacus* bats coincide with periods of increased risk of human infection. PLoS Pathog. *8*, e1002877. https://doi.org/10.1371/journal.ppat.1002877.

Avery, P., Barzilai, N., Benetos, A., Bilianou, H., Capri, M., Caruso, C., Franceschi, C., Katsiki, N., Mikhailidis, D.P., Panotopoulos, G., et al. (2014). Ageing, longevity, exceptional longevity and related genetic and non genetics markers: panel statement. Curr. Vasc. Pharmacol. *12*, 659–661. https://doi.org/10.2174/15701611116613219101226.

Baker, M.L., Schountz, T., and Wang, L.F. (2013). Antiviral immune responses of bats: a review. Zoonoses Public Health *60*, 104–116. https://doi.org/10.1111/j.1863-2378.2012.01528.x.

Banerjee, A., Baker, M.L., Kulcsar, K., Misra, V., Plowright, R., and Mossman, K. (2020). Novel insights into immune systems of bats. Front. Immunol. *11*, 26. https://doi.org/10.3389/fimmu.2020.00026.

Bausch, D.G., Nichol, S.T., Muyembe-Tamfum, J.J., Borchert, M., Rollin, P.E., Sleurs, H., Campbell, P., Tshioko, F.K., Roth, C., Colebunders, R., et al. (2006). Marburg hemorrhagic fever associated with multiple genetic lineages of virus. N. Engl. J. Med. *355*, 909–919. https://doi.org/10.1056/NEJMoa051465.

Becht, E., McInnes, L., Healy, J., Dutertre, C.A., Kwok, I.W.H., Ng, L.G., Ginhoux, F., and Newell, E.W. (2018). Dimensionality reduction for visualizing single-cell data using UMAP. Nat. Biotechnol. *37*, 38–44. https://doi.org/10.1038/nbt.4314.

Becker, D.J., Nachtmann, C., Argibay, H.D., Botto, G., Escalera-Zamudio, M., Carrera, J.E., Tello, C., Winiarski, E., Greenwood, A.D., Méndez-Ojeda, M.L., et al. (2019). Leukocyte profiles reflect geographic range limits in a widespread neotropical bat. Integr. Comp. Biol. *59*, 1176–1189. https://doi.org/10.1093/icb/icz007.

Bondet, V., Le Baut, M., Le Poder, S., Lécu, A., Petit, T., Wedlarski, R., Duffy, D., and Le Roux, D. (2021). Constitutive IFNα protein production in bats. Front. Immunol. *12*, 735866. https://doi.org/10.1101/2021.06.21.449208.

Burny, W., Callegaro, A., Bechtold, V., Clement, F., Delhaye, S., Fissette, L., Janssens, M., Leroux-Roels, G., Marchant, A., van den Berg, R.A., et al. (2017). Different adjuvants induce common innate pathways that are associated with enhanced adaptive responses against a model antigen in humans. Front. Immunol. *8*, 943. https://doi.org/10.3389/fimmu.2017.00943.

Butcher, S.K., Chahal, H., Nayak, L., Sinclair, A., Henriquez, N.V., Sapey, E., O'Mahony, D., and Lord, J.M. (2001). Senescence in innate immune responses: reduced neutrophil phagocytic capacity and CD16 expression in elderly humans. J. Leukoc. Biol. *70*, 881–886.

Büttner, M., Ostner, J., Müller, C.L., Theis, F.J., and Schubert, B. (2021). scCODA is a Bayesian model for compositional single-cell data analysis. Nat. Commun. *12*, 6876. https://doi.org/10.1038/s41467-021-27150-6.

Chakravarty, A.K., and Paul, B.N. (1987). Analysis of suppressor factor in delayed immune responses of a bat, *Pteropus giganteus*. Dev. Comp. Immunol. *11*, 649–660. https://doi.org/10.1016/0145-305x(87)90053-x.

Chakravarty, A.K., and Sarkar, S.K. (1994). Immunofluorescence analysis of immunoglobulin bearing lymphocytes in the Indian fruit bat: *Pteropus giganteus*. Lymphology *27*, 97–104.

Channathodiyil, P., and Houseley, J. (2021). Glyoxal fixation facilitates transcriptome analysis after antigen staining and cell sorting by flow cytometry. PLoS One *16*, e0240769. https://doi.org/10.1371/journal.pone.0240769.

Christensen, J.E., Andreasen, S.O., Christensen, J.P., and Thomsen, A.R. (2001). CD11b expression as a marker to distinguish between recently activated effector CD8(+) T cells and memory cells. Int. Immunol. *13*, 593–600. https://doi.org/10.1093/intimm/13.4.593.

Donath, A., Jühling, F., Al-Arab, M., Bernhart, S.H., Reinhardt, F., Stadler, P.F., Middendorf, M., and Bernt, M. (2019). Improved annotation of protein-coding genes boundaries in metazoan mitochondrial genomes. Nucleic Acids Res. *47*, 10543–10552. https://doi.org/10.1093/nar/gkz833.

Dutertre, C.A., Becht, E., Irac, S.E., Khalilnezhad, A., Narang, V., Khalilnezhad, S., Ng, P.Y., van den Hoogen, L.L., Leong, J.Y., Lee, B., et al. (2019). Single-cell analysis of human mononuclear phagocytes reveals subset-defining markers and identifies circulating inflammatory dendritic cells. Immunity *51*, 573–589.e8. https://doi.org/10.1016/j.immuni.2019.08.008.

Edson, D., Peel, A.J., Huth, L., Mayer, D.G., Vidgen, M.E., McMichael, L., Broos, A., Melville, D., Kristoffersen, J., de Jong, C., et al. (2019). Time of year, age class and body condition predict Hendra virus infection in Australian black flying foxes (Pteropus alecto). Epidemiol. Infect. *147*, e240. https://doi.org/10.1017/S0950268819001237.

Gamage, A.M., Zhu, F., Ahn, M., Foo, R.J.H., Hey, Y.Y., Low, D.H.W., Mendenhall, I.H., Dutertre, C.A., and Wang, L.F. (2020). Immunophenotyping monocytes, macrophages and granulocytes in the Pteropodid bat *Eonycteris spelaea*. Sci. Rep. *10*, 309. https://doi.org/10.1038/s41598-019-57212-1.

Geirsdottir, L., David, E., Keren-Shaul, H., Weiner, A., Bohlen, S.C., Neuber, J., Balic, A., Giladi, A., Sheban, F., Dutertre, C.A., et al. (2019). Cross-species single-cell analysis reveals divergence of the primate microglia program. Cell *179*, 1609–1622.e16. https://doi.org/10.1016/j.cell.2019.11.010.

Goh, G., Ahn, M., Zhu, F., Lee, L.B., Luo, D., Irving, A.T., and Wang, L.-F. (2020). Complementary regulation of caspase-1 and IL-1β reveals additional mechanisms of dampened inflammation in bats. Proc. Natl. Acad. Sci. USA *117*, 28939–28949. https://doi.org/10.1073/pnas.2003352117.

Guito, J.C., Prescott, J.B., Arnold, C.E., Amman, B.R., Schuh, A.J., Spengler, J.R., Sealy, T.K., Harmon, J.R., Coleman-McCray, J.D., Kulcsar, K.A., et al. (2021). Asymptomatic infection of Marburg virus reservoir bats is explained

by a strategy of immunoprotective disease tolerance. Curr. Biol. *31*, 257–270.e5. https://doi.org/10.1016/j.cub.2020.10.015.

Gupta-Wright, A., Tembo, D., Jambo, K.C., Chimbayo, E., Mvaya, L., Caldwell, S., Russell, D.G., and Mwandumba, H.C. (2017). Functional analysis of phagocyte activity in whole blood from HIV/Tuberculosis-Infected individuals using a novel flow cytometry-based assay. Front. Immunol. *8*, 1222. https://doi.org/10.3389/fimmu.2017.01222.

Halpin, K., Hyatt, A.D., Fogarty, R., Middleton, D., Bingham, J., Epstein, J.H., Rahman, S.A., Hughes, T., Smith, C., Field, H.E., et al. (2011). Pteropid bats are confirmed as the reservoir hosts of henipaviruses: a comprehensive experimental study of virus transmission. Am. J. Trop. Med. Hyg. *85*, 946–951. https://doi.org/10.4269/ajtmh.2011.10-0567.

Hathcock, K.S., Hirano, H., Murakami, S., and Hodes, R.J. (1993). CD44 expression on activated B cells. Differential capacity for CD44-dependent binding to hyaluronic acid. J. Immunol. *151*, 6712–6722.

Haug, T., Aigner, M., Peuser, M.M., Strobl, C.D., Hildner, K., Mougiakakos, D., Bruns, H., Mackensen, A., and Völkl, S. (2019). Human double-negative regulatory T-cells induce a metabolic and functional switch in effector T-cells by suppressing mTOR activity. Front. Immunol. *10*, 883. https://doi.org/10.3389/fimmu.2019.00883.

He, X., Korytař, T., Schatz, J., Freuling, C.M., Müller, T., and Köllner, B. (2014). Anti-lyssaviral activity of interferons kappa and omega from the serotine bat, *Eptesicus serotinus*. J. Virol. *88*, 5444–5454. https://doi.org/10.1128/JVI.03403-13.

Hearps, A.C., Martin, G.E., Angelovich, T.A., Cheng, W.J., Maisa, A., Landay, A.L., Jaworowski, A., and Crowe, S.M. (2012). Aging is associated with chronic innate immune activation and dysregulation of monocyte phenotype and function. Aging Cell *11*, 867–875. https://doi.org/10.1111/j.1474-9726.2012.00851.x.

Heaton, H., Talman, A.M., Knights, A., Imaz, M., Gaffney, D.J., Durbin, R., Hemberg, M., and Lawniczak, M.K.N. (2020). Souporcell: robust clustering of single-cell RNA-seq data by genotype without reference genotypes. Nat. Methods *17*, 615–620. https://doi.org/10.1038/s41592-020-0820-1.

Herrera-Uribe, J., Wiarda, J.E., Sivasankaran, S.K., Daharsh, L., Liu, H., Byrne, K.A., Smith, T.P.L., Lunney, J.K., Loving, C.L., and Tuggle, C.K. (2021). Reference transcriptomes of porcine peripheral immune cells created through bulk and single-cell RNA sequencing. Front. Genet. *12*, 689406. https://doi.org/10.3389/fgene.2021.689406.

Hilton, H.G., Rubinstein, N.D., Janki, P., Ireland, A.T., Bernstein, N., Fong, N.L., Wright, K.M., Smith, M., Finkle, D., Martin-McNulty, B., et al. (2019). Single-cell transcriptomics of the naked mole-rat reveals unexpected features of mammalian immunity. PLoS Biol. *17*, e3000528. https://doi.org/10.1371/journal.pbio.3000528.

Ince, L.M., Weber, J., and Scheiermann, C. (2018). Control of leukocyte trafficking by stress-associated hormones. Front. Immunol. *9*, 3143. https://doi.org/10.3389/fimmu.2018.03143.

Irving, A.T., Ahn, M., Goh, G., Anderson, D.E., and Wang, L.-F. (2021). Lessons from the host defences of bats, a unique viral reservoir. Nature *589*, 363–370. https://doi.org/10.1038/s41586-020-03128-0.

Jacques Dainat, D.H., and Pascal, P. (2021). NBISweden/AGAT: AGAT-v0.6.2 (v0.6.2).

Jebb, D., Huang, Z., Pippel, M., Hughes, G.M., Lavrichenko, K., Devanna, P., Winkler, S., Jermiin, L.S., Skirmuntt, E.C., Katzourakis, A., et al. (2020). Six reference-quality genomes reveal evolution of bat adaptations. Nature *583*, 578–584. https://doi.org/10.1038/s41586-020-2486-3.

Kandeil, A., Gomaa, M.R., Shehata, M.M., El Taweel, A.N., Mahmoud, S.H., Bagato, O., Moatasim, Y., Kutkat, O., Kayed, A.S., Dawson, P., et al. (2019). Isolation and characterization of a distinct influenza A virus from Egyptian bats. J. Virol. *93*, e01059-18. https://doi.org/10.1128/JVI.01059-18.

Keresztes, M., Rudisch, T., Tajti, J., Ocsovszki, I., and Gardi, J. (2007). Granulocyte activation in humans is modulated by psychological stress and relaxation. Stress *10*, 271–281. https://doi.org/10.1080/10253890701248079.

Kingston, T., Aguirre, L., Armstrong, K., Mies, R., Racey, P., Rodríguez-Herrera, B., and Waldien, D. (2016). Networking networks for global bat conservation. In Bats in the Anthropocene: Conservation of Bats in a Changing World, C.C. Voigt and T. Kingston, eds. (Springer International Publishing), pp. 539–569. https://doi.org/10.1007/978-3-319-25220-9_17.

Kollmann, T.R., Kampmann, B., Mazmanian, S.K., Marchant, A., and Levy, O. (2017). Protecting the newborn and young infant from infectious diseases: lessons from immune ontogeny. Immunity *46*, 350–363. https://doi.org/10.1016/j.immuni.2017.03.009.

Kunz, T.H. (1982). Ecology of Bats (Springer US).

La Manno, G., Gyllborg, D., Codeluppi, S., Nishimura, K., Salto, C., Zeisel, A., Borm, L.E., Stott, S.R.W., Toledo, E.M., Villaescusa, J.C., et al. (2016). Molecular diversity of midbrain development in mouse, human, and stem cells. Cell *167*, 566–580.e19. https://doi.org/10.1016/j.cell.2016.09.027.

Larson, P.A., Bartlett, M.L., Garcia, K., Chitty, J., Balkema-Buschmann, A., Towner, J., Kugelman, J., Palacios, G., and Sanchez-Lockhart, M. (2021). Genomic features of humoral immunity support tolerance model in Egyptian rousette bats. Cell Rep. *35*, 109140. https://doi.org/10.1016/j.celrep.2021.109140.

Lee, A.K., Kulcsar, K.A., Elliott, O., Khiabanian, H., Nagle, E.R., Jones, M.E.B., Amman, B.R., Sanchez-Lockhart, M., Towner, J.S., Palacios, G., and Rabadan, R. (2015). *De novo* transcriptome reconstruction and annotation of the Egyptian rousette bat. BMC Genom. *16*, 1033. https://doi.org/10.1186/s12864-015-2124-x.

Markovic, S.N., Knight, P.R., and Murasko, D.M. (1993). Inhibition of interferon stimulation of natural killer cell activity in mice anesthetized with halothane or isoflurane. Anesthesiology *78*, 700–706. https://doi.org/10.1097/00000542-199304000-00013.

Martínez Gómez, J.M., Periasamy, P., Dutertre, C.A., Irving, A.T., Ng, J.H.J., Crameri, G., Baker, M.L., Ginhoux, F., Wang, L.F., and Alonso, S. (2016). Phenotypic and functional characterization of the major lymphocyte populations in the fruit-eating bat *Pteropus alecto*. Sci. Rep. *6*, 37796. https://doi.org/10.1038/srep37796.

McFarland, H.I., Nahill, S.R., Maciaszek, J.W., and Welsh, R.M. (1992). CD11b (Mac-1): a marker for CD8+ cytotoxic T cell activation and memory in virus infection. J. Immunol. *149*, 1326–1333.

Middleton, D.J., Morrissy, C.J., van der Heide, B.M., Russell, G.M., Braun, M.A., Westbury, H.A., Halpin, K., and Daniels, P.W. (2007). Experimental Nipah virus infection in pteropid bats (*Pteropus poliocephalus*). J. Comp. Pathol. *136*, 266–272. https://doi.org/10.1016/j.jcpa.2007.03.002.

Moore, P.R., Jansen, C.C., Graham, G.C., Smith, I.L., and Craig, S.B. (2010). Emerging tropical diseases in Australia. Part 3. Australian bat lyssavirus. Ann. Trop. Med. Parasitol. *104*, 613–621. https://doi.org/10.1179/136485910X12851868779948.

Munster, V.J., Adney, D.R., van Doremalen, N., Brown, V.R., Miazgowicz, K.L., Milne-Price, S., Bushmaker, T., Rosenke, R., Scott, D., Hawkinson, A., et al. (2016). Replication and shedding of MERS-CoV in Jamaican fruit bats (*Artibeus jamaicensis*). Sci. Rep. *6*, 21878. https://doi.org/10.1038/srep21878.

Nowak, R.M., and Walker, E.P. (1994). Walker's Bats of the World (Johns Hopkins University Press).

Papenfuss, A.T., Baker, M.L., Feng, Z.P., Tachedjian, M., Crameri, G., Cowled, C., Ng, J., Janardhana, V., Field, H.E., and Wang, L.F. (2012). The immune gene repertoire of an important viral reservoir, the Australian black flying fox. BMC Genom. *13*, 261. https://doi.org/10.1186/1471-2164-13-261.

Park, C.K., Shin, Y.K., Kim, T.J., Park, S.H., and Ahn, G.H. (1999). High CD99 expression in memory T and B cells in reactive lymph nodes. J. Kor. Med. Sci. *14*, 600–606. https://doi.org/10.3346/jkms.1999.14.6.600.

Patel, R.S., Tomlinson, J.E., Divers, T.J., Van de Walle, G.R., and Rosenberg, B.R. (2021). Single-cell resolution landscape of equine peripheral blood mononuclear cells reveals diverse cell types including T-bet(+) B cells. BMC Biol. *19*, 13. https://doi.org/10.1186/s12915-020-00947-5.

Pavlovich, S.S., Lovett, S.P., Koroleva, G., Guito, J.C., Arnold, C.E., Nagle, E.R., Kulcsar, K., Lee, A., Thibaud-Nissen, F., Hume, A.J., et al. (2018). The

Egyptian rousette genome reveals unexpected features of bat antiviral immunity. Cell *173*, 1098–1110.e18. https://doi.org/10.1016/j.cell.2018.03.070.

Paweska, J.T., Storm, N., Grobbelaar, A.A., Markotter, W., Kemp, A., and Jansen van Vuren, P. (2016). Experimental inoculation of Egyptian fruit bats (*Rousettus aegyptiacus*) with Ebola virus. Viruses *8*. https://doi.org/10.3390/v8020029.

Periasamy, P., Hutchinson, P.E., Chen, J., Bonne, I., Shahul Hameed, S.S., Selvam, P., Hey, Y.Y., Fink, K., Irving, A.T., Dutertre, C.A., et al. (2019). Studies on B Cells in the fruit-eating black flying fox (*Pteropus alecto*). Front. Immunol. *10*, 489. https://doi.org/10.3389/fimmu.2019.00489.

Piątosa, B., Wolska-Kuśnierz, B., Pac, M., Siewiera, K., Gałkowska, E., and Bernatowska, E. (2010). B cell subsets in healthy children: reference values for evaluation of B cell maturation process in peripheral blood. Cytometry B Clin. Cytom. *78*, 372–381. https://doi.org/10.1002/cyto.b.20536.

Plowden, J., Renshaw-Hoelscher, M., Engleman, C., Katz, J., and Sambhara, S. (2004). Innate immunity in aging: impact on macrophage function. Aging Cell *3*, 161–167. https://doi.org/10.1111/j.1474-9728.2004.00102.x.

Ren, L., Wu, C., Guo, L., Yao, J., Wang, C., Xiao, Y., Pisco, A.O., Wu, Z., Lei, X., Liu, Y., et al. (2020). Single-cell transcriptional atlas of the Chinese horseshoe bat (Rhinolophus sinicus) provides insight into the cellular mechanisms which enable bats to be viral reservoirs. Preprint at biorxiv. https://doi.org/10.1101/2020.06.30.175778.

Sarkar, S.K., and Chakravarty, A.K. (1991). Analysis of immunocompetent cells in the bat, *Pteropus giganteus*: isolation and scanning electron microscopic characterization. Dev. Comp. Immunol. *15*, 423–430. https://doi.org/10.1016/0145-305x(91)90034-v.

Satija, R., Farrell, J.A., Gennert, D., Schier, A.F., and Regev, A. (2015). Spatial reconstruction of single-cell gene expression data. Nat. Biotechnol. *33*, 495–502. https://doi.org/10.1038/nbt.3192.

Simell, B., Vuorela, A., Ekström, N., Palmu, A., Reunanen, A., Meri, S., Käyhty, H., and Väkeväinen, M. (2011). Aging reduces the functionality of anti-pneumococcal antibodies and the killing of *Streptococcus pneumoniae* by neutrophil phagocytosis. Vaccine *29*, 1929–1934. https://doi.org/10.1016/j.vaccine.2010.12.121.

Simon, A.K., Hollander, G.A., and McMichael, A. (2015). Evolution of the immune system in humans from infancy to old age. Proc. Biol. Sci. *282*, 20143085. https://doi.org/10.1098/rspb.2014.3085.

Stewart, A., Ng, J.C.F., Wallis, G., Tsioligka, V., Fraternali, F., and Dunn-Walters, D.K. (2021). Single-cell transcriptomic analyses define distinct peripheral B cell subsets and discrete development pathways. Front. Immunol. *12*, 602539. https://doi.org/10.3389/fimmu.2021.602539.

Storm, N., Jansen Van Vuren, P., Markotter, W., and Paweska, J.T. (2018). Antibody responses to Marburg virus in Egyptian rousette bats and their role in protection against infection. Viruses *10*, E73. https://doi.org/10.3390/v10020073.

Stuart, T., Butler, A., Hoffman, P., Hafemeister, C., Papalexi, E., Mauck, W.M., 3rd, Hao, Y., Stoeckius, M., Smibert, P., and Satija, R. (2019). Comprehensive integration of single-cell data. Cell *177*, 1888–1902.e21. https://doi.org/10.1016/j.cell.2019.05.031.

Swanepoel, R., Smit, S.B., Rollin, P.E., Formenty, P., Leman, P.A., Kemp, A., Burt, F.J., Grobbelaar, A.A., Croft, J., Bausch, D.G., et al. (2007). Studies of reservoir hosts for Marburg virus. Emerg. Infect. Dis. *13*, 1847–1851. https://doi.org/10.3201/eid1312.071115.

Timen, A., Koopmans, M.P.G., Vossen, A.C.T.M., van Doornum, G.J.J., Günther, S., van den Berkmortel, F., Verduin, K.M., Dittrich, S., Emmerich, P., Osterhaus, A.D.M.E., et al. (2009). Response to imported case of Marburg hemorrhagic fever, The Netherlands. Emerg. Infect. Dis. *15*, 1171–1175. https://doi.org/10.3201/eid1508.090051.

Towner, J.S., Amman, B.R., Sealy, T.K., Carroll, S.A.R., Comer, J.A., Kemp, A., Swanepoel, R., Paddock, C.D., Balinandi, S., Khristova, M.L., et al. (2009). Isolation of genetically diverse Marburg viruses from Egyptian fruit bats. PLoS Pathog. *5*, e1000536. https://doi.org/10.1371/journal.ppat.1000536.

Towner, J.S., Pourrut, X., Albariño, C.G., Nkogue, C.N., Bird, B.H., Grard, G., Ksiazek, T.G., Gonzalez, J.P., Nichol, S.T., and Leroy, E.M. (2007). Marburg virus infection detected in a common African bat. PLoS One *2*, e764. https://doi.org/10.1371/journal.pone.0000764.

Traag, V.A., Waltman, L., and van Eck, N.J. (2019). From Louvain to Leiden: guaranteeing well-connected communities. Sci. Rep. *9*, 5233. https://doi.org/10.1038/s41598-019-41695-z.

Valiathan, R., Ashman, M., and Asthana, D. (2016). Effects of ageing on the immune system: infants to elderly. Scand. J. Immunol. *83*, 255–266. https://doi.org/10.1111/sji.12413.

Van Der Westhuyzen, J. (1988). Haematology and iron status of the egyptian fruit bat, *rousettus aegyptiacus*. Comp. Biochem. Physiol. A Comp. Physiol. *90*, 117–120. https://doi.org/10.1016/0300-9629(88)91015-8.

Vidgen, M.E., de Jong, C., Rose, K., Hall, J., Field, H.E., and Smith, C.S. (2015). Novel paramyxoviruses in Australian flying-fox populations support host-virus co-evolution. J. Gen. Virol. *96*, 1619–1625. https://doi.org/10.1099/vir.0.000099.

Wang, L.F., Gamage, A.M., Chan, W.O.Y., Hiller, M., and Teeling, E.C. (2021). Decoding bat immunity: the need for a coordinated research approach. Nat. Rev. Immunol. *21*, 269–271. https://doi.org/10.1038/s41577-021-00523-0.

Watanabe, S., Masangkay, J.S., Nagata, N., Morikawa, S., Mizutani, T., Fukushi, S., Alviola, P., Omatsu, T., Ueda, N., Iha, K., et al. (2010). Bat coronaviruses and experimental infection of bats, the Philippines. Emerg. Infect. Dis. *16*, 1217–1223. https://doi.org/10.3201/eid1608.100208.

Watt, S.M., Burgess, A.W., Metcalf, D., and Battye, F.L. (1980). Isolation of mouse bone marrow neutrophils by light scatter and autofluorescence. J. Histochem. Cytochem. *28*, 934–946. https://doi.org/10.1177/28.9.7410816.

Wein, A.N., McMaster, S.R., Takamura, S., Dunbar, P.R., Cartwright, E.K., Hayward, S.L., McManus, D.T., Shimaoka, T., Ueha, S., Tsukui, T., et al. (2019). CXCR6 regulates localization of tissue-resident memory CD8 T cells to the airways. J. Exp. Med. *216*, 2748–2762. https://doi.org/10.1084/jem.20181308.

Wenisch, C., Patruta, S., Daxböck, F., Krause, R., and Hörl, W. (2000). Effect of age on human neutrophil function. J. Leukoc. Biol. *67*, 40–45. https://doi.org/10.1002/jlb.67.1.40.

Williamson, M.M., Hooper, P.T., Selleck, P.W., Gleeson, L.J., Daniels, P.W., Westbury, H.A., and Murray, P.K. (1998). Transmission studies of Hendra virus (equine morbillivirus) in fruit bats, horses and cats. Aust. Vet. J. *76*, 813–818. https://doi.org/10.1111/j.1751-0813.1998.tb12335.x.

Williamson, M.M., Hooper, P.T., Selleck, P.W., Westbury, H.A., and Slocombe, R.F. (2000). Experimental hendra virus infectionin pregnant Guinea-pigs and fruit Bats (*Pteropus poliocephalus*). J. Comp. Pathol. *122*, 201–207. https://doi.org/10.1053/jcpa.1999.0364.

Xie, J., Li, Y., Shen, X., Goh, G., Zhu, Y., Cui, J., Wang, L.-F., Shi, Z.-L., and Zhou, P. (2018). Dampened STING-dependent interferon activation in bats. Cell Host Microbe *23*, 297–301.e4. https://doi.org/10.1016/j.chom.2018.01.006.

Zhang, G., Cowled, C., Shi, Z., Huang, Z., Bishop-Lilly, K.A., Fang, X., Wynne, J.W., Xiong, Z., Baker, M.L., Zhao, W., et al. (2013). Comparative analysis of bat genomes provides insight into the evolution of flight and immunity. Science *339*, 456–460. https://doi.org/10.1126/science.1230835.

Zhou, P., Chionh, Y.T., Irac, S.E., Ahn, M., Jia Ng, J.H., Fossum, E., Bogen, B., Ginhoux, F., Irving, A.T., Dutertre, C.A., and Wang, L.F. (2016a). Unlocking bat immunology: establishment of *Pteropus alecto* bone marrow-derived dendritic cells and macrophages. Sci. Rep. *6*, 38597. https://doi.org/10.1038/srep38597.

Zhou, P., Tachedjian, M., Wynne, J.W., Boyd, V., Cui, J., Smith, I., Cowled, C., Ng, J.H.J., Mok, L., Michalski, W.P., et al. (2016b). Contraction of the type I IFN locus and unusual constitutive expression of IFN-α in bats. Proc. Natl. Acad. Sci. USA *113*, 2696–2701. https://doi.org/10.1073/pnas.1518240113.

STAR★METHODS

KEY RESOURCES TABLE

REAGENT or RESOURCE	SOURCE	IDENTIFIER
Antibodies		
Goat anti-mouse IgG1, BV421	BioLegend	#405317; RRID: AB_10900419
Mouse anti-human CD79a, PerCP-Cy5.5	BioLegend	#333508; RRID: AB_2075752
Mouse anti-bovine CD172a	Bio-Rad	#MCA6079
Mouse anti-human CD206, PE-Cy-7	BioLegend	#321124; RRID: AB_10933248
Mouse anti-human Ki-67, BV786	BD Biosciences	#563756; RRID: AB_2732007
Rat anti-human CD3ε, Pacific Blue	Bio-Rad	#MCA1477PB; RRID: AB_10843429
Rat anti-human/mouse CD11b, BV711	BioLegend	#101242; RRID: AB_2563310
Rat anti-mouse I-Ad/I-Ed (MHCII), PE	BD Biosciences	#558593; RRID: AB_647221
Chemicals, peptides, and recombinant proteins		
β-mercaptoethanol	Gibco	# 21985023
CellTrace™ CFSE	Invitrogen	#C34554
Collagenase IV	Worthington Biochemical Corporation	#LS004186
Concanavalin A (ConA)	Sigma-Aldrich	#C0412
DNaseI	Roche	#9003-98-9
EDTA	Roth	#8043.2
Endotoxin-free water	Sigma-Aldrich	# TMS-011-A
Escherichia coli (K-12 strain) BioParticles™, Fluorescein conjugated	Invitrogen	#E2861
Ficoll® Paque PLUS	Cytiva	# 17144003
Glyoxal solution 40%	Sigma-Aldrich	# 128465
HEPES	Gibco	# 11560496
L-Glutamine	Gibco	# A2916801
Lipopolysaccharide (LPS)	Sigma-Aldrich	#L6529-1MG
DPBS	Thermo Fisher Scientific	# 14190144
Red Blood Cell Lysis Buffer (10X)	BioLegend	#420302
Staphylococcal Enterotoxin B (SEB)	Sigma-Aldrich	#S4881-1MG
UltraPure™ BSA	Thermo Fisher Scientific	#AM2618
Critical commercial assays		
Chromium i7 Multiplex Kit, 96 rxns	10× Genomics	#PN-120262
Chromium Single Cell 3' GEM, Library & Gel Bead Kit v3, 4 rxns	10× Genomics	#PN-1000092
Chromium Single Cell B Chip Kit, 16 rxns	10× Genomics	#PN-1000074
DiffQuick Kit	Fisher Scientific	# 10435310
GoTaq® DNA Polymerase	Promega	#M3001
LunaScript® RT SuperMix Kit	New England BioLabs	#E3010L
QIAquick Gel Extraction Kit	Qiagen	# 28704
True-Nuclear™ Transcription Factor Buffer Set	BioLegend	#424401
Zombie Aqua™ Fixable Viability Kit	BioLegend	#423102
Deposited data		
scRNA-seq expression data, browsable	This paper	GEO (GSE183925)
R and Python based analysis of expression data	This paper	https://github.com/Christophe29-BZH/ImmuBat_ERB_Blood

(*Continued on next page*)

Continued

REAGENT or RESOURCE	SOURCE	IDENTIFIER
Experimental models: Organisms/strains		
Rousettus aegyptiacus: Adult (n = 28, 3-6 years of age) Subadult (n = 6, 1-2 years old) Juvenile (n = 32, $\leq$ 1 year of age) Institutional permission: LALLF 7221.3-2-042/17	FLI breeding colony	N/A
Oligonucleotides		
For all oligonucleotide sequences, refer to Table S5.	This paper, Eurofins	PMID of reference gene oligonucleotides: 34737406
Software and algorithms		
AGAT version 0.8.0	Jacques Dainat	https://github.com/NBISweden/AGAT
BioRender	BioRender Company	RRID: SCR_018361 https://biorender.com/
Cellranger version 3.1.0	10× Genomics	RRID: SCR_017344 https://support.10xgenomics.com/single-cell-gene-expression
FACS DIVA Software 9.0.1	BD Biosciences	RRID: SCR_001456
FlowJo 10.5.3	BD Biosciences	RRID: SCR_008520 https://www.flowjo.com/
Geneious Prime 2021.0.1	Biomatters	RRID: SCR_010519
MITOS version 2	Donath et al. (2019)	http://mitos2.bioinf.uni-leipzig.de/index.py
Nucleotide and Protein BLAST	NCBI	RRID: SCR_004870 https://blast.ncbi.nlm.nih.gov/Blast.cgi
OligoAnalyzer Tool	Integrated DNA Technologies	RRID: SCR_001363 https://eu.idtdna.com/pages/tools/oligoanalyzer?returnurl=%2Fcalc%2Fanalyzer
PrimerQuest	Integrated DNA Technologies	https://eu.idtdna.com/pages/tools/primerquest?returnurl=%2FPrimerQuest%2FHome%2FIndex
Prism 9.0.0	GraphPad Software	RRID: SCR_002798 https://www.graphpad.com/scientific-software/prism/
Python version 3.9.7	Python Software Foundation	RRID:SCR_008394 https://www.python.org/
R package Seurat version 4.0	Satija et al. (2015)	RRID:SCR_016341 https://satijalab.org/seurat/
R package Leidenbase version 0.1.3	Cole Trapnell lab	https://github.com/cole-trapnell-lab/leidenbase
R version 4.0.3	R Core Team	RRID:SCR_000432 https://www.r-project.org/
scCODA version 0.1.7	Buttner et al. (2021)	https://sccoda.readthedocs.io/en/latest/
Souporcell version 2.0	Heaton et al. (2020)	https://github.com/wheaton5/souporcell
Other		
100 μm Cell strainers	Fisher Scientific	#128704
Flowmi® Cell strainers	Sigma-Aldrich	#BAH136800040
Protein LoBind™ reaction tubes 1.5 mL	Eppendorf	#0030108116
TubeSeq Service	Eurofins	N/A

RESOURCE AVAILABILITY

Lead contact

Further information and requests for resources and reagents should be directed to and will be fulfilled by the lead contact, Anca Dorhoi (anca.dorhoi@fli.de).

Materials availability

This study did not generate new unique reagents.

Data and code availability

- scRNA-seq datasets that were generated for this study have been deposited in Gene Expression Omnibus (GEO: GSE183925). All scRNA-seq expression data can be browsed on a user-friendly dedicated webinterface: https://infection-atlas.org/Immubat-ERB-Blood/.
- R and python scripts used for analysis of the scRNA-seq data are available on GitHub: https://github.com/Christophe29-BZH/ImmuBat_ERB_Blood
- Any additional information required to reanalyze the data reported in this paper is available from the lead contact upon request.

EXPERIMENTAL MODEL AND SUBJECT DETAILS

Animals and animal housing

Male and female ERB were kept in captive breeding colonies of 20m^2 per aviary under quarantine conditions according to current German Animal Welfare Regulations. Bats were classified as adult (3-6 years of age, n = 28), subadult (1-2 years old, n = 6) and juvenile ($\leq$1 year of age, n = 32) and were kept in colonies of approx. 20 animals per room in a Biosafety Level 1 facility, at 24-26°C and 60-70% humidity, and light between 6 am and 6 pm including a dimming phase. Diet comprises varying fruits and vegetables. Only limited number of staff have access to the rooms, encouraging bats to trust known caretakers in order to reduce stress level. Sampling and necropsies were approved by the local authorities (LALLF 7221.3-2-042/17). All experiments were carried out according to ARRIVE guidelines (https://arriveguidelines.org) and each group/room is represented equally in the data presented in this study.

METHOD DETAILS

Blood and tissue sampling

Peripheral blood from male and female ERB was obtained during short time sedation with Isoflurane (CP Pharma) and puncture of the uropatagial vein. 4 adult and 4 juvenile ERB females were euthanized and afterward lung, spleen and mLNs were immediately collected for cell enrichment. Samples from 12 adult and 10 juvenile ERB were subjected to phenotyping via flow cytometry. Samples from additional 11 adult (older than three years) and juvenile (around one year of age) ERB were used for assessment of granulocyte frequencies. For scRNA-seq of whole blood, samples from 4 adult, 2 subadults and 3 juvenile ERB were used; scRNA-seq of ERB PBMC was carried out with samples from one adult and two subadult ERB. Mostly female ERB were used in this study, which is due to the natural ratio of male to female bats within a colony. The FLI breeding colony is maintained according to wild counterparts, where few adult dominant males are present. To ensure successful breeding and genepool diversity, adult males were not subjected to necropsy.

Tissue preparation

Single cell suspensions from spleen and mLNs were obtained by carefully grinding the tissue through a 100 μm cell strainer (Fisher Scientific) with ice-cold homemade PBS supplemented with 0.5% EDTA (Roth) (PBS-EDTA). Lung tissue was cut into small pieces and digested with 800 μg/mL Collagenase IV (Worthington Biochemical Corporation) and 125 μg/mL DNAse I (Roche) in serum-free DMEM. The mixture was incubated at 37°C for 1 h, diluted in PBS-EDTA and filtered through a 100 μm cell strainer. Single cell suspensions were centrifuged at 350 ×g for 15 min at 4°C and pellets were resuspended in PBS-EDTA or FACS buffer (PBS, 0.1% EDTA, 1% murine serum, 1% rat serum, 1% fetal-calf serum (FCS)).

Processing of blood cells for scRNA-seq

300 μL of ERB whole blood was collected and directly subjected to RBC lysis using 10X RBC lysis buffer (BioLegend) diluted 1:10 in endotoxin-free water (Sigma-Aldrich). All washing steps were carried out in DPBS without calcium and magnesium (Thermo Fisher Scientific), supplemented with 20 μg/mL UltraPure™ BSA (Thermo Fisher Scientific). For PBMC isolation, 400 μL of whole blood was each diluted in PBS with 20 μg/mL BSA. Diluted blood was added to 3 mL Ficoll-Paque PLUS (1.077 g/mL, Cytiva) and centrifuged at 760 ×g for 30 min without brakes or acceleration. PMBCs were collected and washed with PBS with 20 μg/mL BSA. Cells were filtered through 70 μm Flowmi® cell strainers (Sigma Aldrich) and sorted with a 100 μm nozzle to deplete platelets using the lowest flow rate and the single cell setting of the cell sorter FACSAria Fusion (BD Biosciences). Cells sorted in Protein LoBind tubes (Eppendorf) pre-coated with FCS were kept on ice until sample collection was complete and subsequently centrifuged at 400 ×g and 4°C for 15 min. After centrifugation, the cell count was set at 1000 cells/μL in 1xPBS +20 μg/mL UltraPure™ BSA. A small aliquot was used to determine cell viability.

Chromium GEM and library generation for scRNA-seq

Chromium Next GEM Single Cell 3′ Reagents Kits v3.1 were used to generate libraries for sequencing. A total of 13,000 cells was added to each well and the manufacturer's protocol was followed. All material needed for single cell sequencing, but not provided in the kits, was obtained according to recommendations from 10× Genomics.

Sequencing of scRNA-seq libraries, data pre-processing and custom cellranger genome generation

All Next GEM Single Cell 3′ v3.1 (10× Genomics) libraries were sequenced as multiplexed pools on an Illumina NovaSeq 6000 in paired-end mode (28 cycles for Read 1 and 91 cycles for Read 2). To pre-process sequencing data, we used the pipelines included in Cellranger (v3.1.0, 10× Genomics). Raw sequencing data were demultiplexed and converted to fastq files with *cellranger mkfastq* and default parameters. Mapping to the reference genome, UMI counting and generation of the gene expression matrices were performed with *cellranger count* and default parameters. We chose a recently published genome of *R. aegyptiacus* with extensive gene annotation as reference for *cellranger count* (RefSeq accession: GCF_014176215.1 (Jebb et al., 2020)). To enrich it for scRNA-seq analysis, we also used the mitochondrial genomic sequence provided by the same authors (GenBank accession: CM024382.1), subjected it to automatic annotation by MITOS (Donath et al., 2019) and converted the output bed file to a gene annotation gtf file with AGAT (Jacques Dainat and Pascal 2021). To ensure compatibility with Cellranger, the obtained mitochondrial gtf file had to be modified manually, first to add exonic features covering the whole genes, second to keep only the 3′ end of CO1 since this gene was overlapping both "ends" of the mitochondrial "chromosome". Finally, both genomic files from *R. aegyptiacus* and mitochondrial genomes and both gtf files were concatenated together and inputed to *cellranger mkref* to generate a Cellranger-compatible genome.

In silico analysis

Protein sequences from *R. aegyptiacus* [Raegyp2.0], the house mouse (*Mus musculus*, GRCm39) and human (*Homo sapiens*, GRCh38.p13) were obtained from the NCBI database. Sequence alignment and consensus analysis was performed using ClustalW alignment in Geneious Prime, Version 2021.0.1 by Biomatters.

Validation of antibody specificity

Blood samples of ERB females were stained and $CD11b^+$ cells, $CD172a^+$cells, granulocytes and corresponding negative populations were purified using the FACSAria Fusion cell sorter (BD Biosciences). To ensure successful RNA extraction after fixation, sorted $CD3^+$ and $CD79a^+$ cells were fixed with a 3% glyoxal solution, pH 4-5 (prepared from 40% glyoxal (Sigma-Aldrich) and stained as described elsewhere (Channathodiyil and Houseley, 2021)). For myeloid cells, droplets of 20 μL cell suspension were carefully placed on a glass slide and subsequently stained with DiffQuick Kit (Fisher Scientific), following manufacturer's instructions. Cells were visualized using a Nikon microscope and 100X magnification. To investigate immune cell marker expression, sorted cells were lysed with homemade Trizol; the RNA was extracted according to the ThermoSci protocol and subsequently transcribed into cDNA using a LunaScript RT SuperMix Kit (New England BioLabs). PCR reactions were carried out using a GoTaq Flexi DNA Polymerase Kit (Promega). Primers were designed and screened for secondary structures using the PrimerQuest and OligoAnalyzer Tools (Integrated DNA Technologies), sequences are listed in Table S5. To confirm amplicon identity, bands were cut and products purified using the QIAquick Gel Extraction Kit (Qiagen) following manufacturer's instructions with exception of eluting DNA from the column membrane with buffer heated to 37°C rather than room temperature. Purified products were subsequently sequenced (Eurofins TubeSeq Service) and results aligned to corresponding sequences in the NCBI database.

Blood smears

One droplet of whole blood per animal (adult $n = 7$, juvenile $n = 9$) was directly processed on a glass slide and stained with the DiffQuick Kit according to manufacturer's instructions. The cells were analysed with a Nikon Eclipse TS2 microscope (Nikon) and a 100X objective. At least 100 cells per slide were counted and cells were identified based on their morphological properties and size.

Flow cytometry

Cells and whole blood were washed with FACS buffer. All centrifugation steps were carried out at 350 ×g for 5 min at 4°C and all incubation steps were performed at 4°C in the dark for 15 min unless stated otherwise. Antibodies used for cell-surface staining are indicated in the KRT and Table S6. Fixable viability dye Zombie Aqua (BioLegend) was included to identify dead cells. RBC lysis was performed on whole blood and organ samples containing a visible amount of erythrocytes using a validated lysis buffer (1.55 M NH_4Cl, 12.7 mM Na_4EDTA, 100 mM $KHCO_3$, pH 7.4 in double distilled water). Prior to intracellular staining, cells were fixed using the True-Nuclear Transcription Factor Buffer Set (BioLegend) and incubated with antibodies for 30 min at 4°C. Samples and data was acquired on a BD LSRFortessa Cytometer, running with FACS DIVA 9.0.1 Software (BD Biosciences) and analyzed using FlowJo 10.5.3 software (BD Biosciences).

Phagocytosis assay

Whole blood was diluted 1:1 with RPMI-1640 supplemented with 2% FCS, 1% HEPES (Gibco), 0.05% β-mercaptoethanol (Gibco) and 1% L-Glutamine (Gibco). Fluorescein-labeled *E. coli* bioparticles (Invitrogen) were processed according to vendor's instructions and cells were incubated under rocking at 37°C for 10 min and 60 min, respectively. Samples were subjected to cell surface and intracellular staining for subsequent flow cytometry measurements.

Mitogenic cell stimulation

PBMC and splenocytes were purified using Ficoll-Paque PLUS (Cytiva) according to manufacturer's protocol. Afterwards, cells were washed with cold PBS-EDTA. To track proliferation, cells were labeled with CFSE (Invitrogen). $CFSE^{low}$ cells or $Ki\text{-}67^+$ cells were

defined as proliferating cells. PBMCs and splenocytes were washed and incubated with either 5 μg/mL ConA (Sigma), 5 μg/mL LPS (Sigma), 100 ng/mL SEB (Sigma) or DMEM as a control for 5 days at 37°C. All cells were collected and subjected to intracellular staining including proliferation marker Ki-67 as well as T and B cell markers for subsequent flow cytometry measurements.

QUANTIFICATION AND STATISTICAL ANALYSIS

Analysis of scRNA-seq data

Individual demultiplexing

Since each library consists of a cell mixture from 3 individuals, we used Souporcell to determine the donor origin of each single cell (Heaton et al., 2020). Briefly, Souporcell relies on the detection of genetic variants as of single nucleotides polymorphisms, to infer genotypes present in the cell mixture. Each single cell can be attributed to a particular individual afterwards. Cell doublets detected by Souporcell were leveraged to identify biases during downstream analysis. In addition, we assigned a sex to each individual based on the expression patterns of *LOC107502967*, *LOC107506326* and *LOC107502043* (putative genes for *XIST*, *TMSB4Y* and *DDX3Y* respectively).

Dataset integration

We used the popular Seurat package for R (v4.0 (Satija et al., 2015)) as our basic framework for scRNA-seq analysis. Prior to integration, genes detected in less than 3 cells and cells with less than 200 detected genes were excluded. The gene expression matrixes from all four libraries were merged together within a single Seurat object. We followed the integration workflow implemented in Seurat to integrate together the data from all 9 individuals and mitigate inter-individual specificities that might obscure the identification of shared cell types (Stuart et al., 2019). Briefly, the dataset was split based on the 9 individuals identified by Souporcell (4× adults, 2× subadults and 3× juveniles). UMI counts were scaled by a 10,000 factor and log-normalized. The 3,000 most highly variable genes (HVGs) were identified for each individual and HVGs detected repeatedly across the different individuals were used as anchor for the integration.

Dimensionality reduction and visualization

Log-normalized counts of HVGs used for integration were scaled before performing principal component analysis (PCA) to capture the principal components (PCs) explaining the highest amount of variation in the data. The top 25 PCs were further compacted into 2 dimensions by UMAP (Becht et al., 2018) for visualization.

Clustering

We applied a graph-based unsupervised machine learning procedure to identify group of single cells with similar transcriptomes, i. e. clusters. Briefly, the top 25 PCs were used to build a KNN graph (k = 20) followed by detection of highly inter-connected group of cells by the Leiden algorithm (Traag et al., 2019). We used the C implementation for R of the Leiden algorithm (leidenbase v0.1.3, Trapnell Lab) with a resolution set at 0.003. Clustering results were used to label cells on the UMAP representation.

Separated analysis of myeloid and lymphoid cells

After establishing the myeloid or lymphoid filiation for each cluster identified in the full dataset, we separated cells from both lineage and repeated the scRNA-seq analysis workflow to obtain a finer cluster resolution. The integration procedure was rerun with 2000 HVGs for myeloid cells and 3000 HVGs for lymphoid cells. The top 12 and 18 PCs were kept after dimensionality reduction for UMAP and clustering, while the resolution parameter of the Leiden algorithm was set to 0.003 or 0.002, respectively for the myeloid and lymphoid cells.

Reclustering of T cell clusters

To focus on T cell subsets, we excluded cells from the B cells, NK-like and Cycling lymphocytes clusters in the lymphoid compartment and repeated the scRNA-seq analysis workflow. The integration procedure was rerun with the top 1,500 HVGs. The top 10 PCs were kept to build the KNN graph (k = 15). Clustering was performed with Leiden (resolution = 0.025) and results were included in the lymphoid UMAP.

Differential gene expression testing

To identify gene markers of each cluster, we performed a Wilcoxon Rank-Sum Test through the *FindAllMarkers* function of Seurat. Only upregulated genes that were expressed in at least 20% of the cells from a given cluster, with a log2 fold-change > 0.5 compared to the average expression in cells from all other clusters and a Bonferroni corrected p-value < 0.05 were considered as differentially expressed. Since this approach is sensitive to the composition of the dataset and mainly allows the detection of the most obvious gene markers, we also performed pairwise tests through the *FindMarkers* function when investigating fine differences between clusters from a same putative cell type. Putative annotations inferred from DEGs were used to label clusters on the UMAP representations.

Compositional analysis across ages

For compositional analysis, we used the recently reported scCODA framework (Buttner et al., 2021) to test for differentially abundant cell clusters in the blood of adult, subadult and juvenile ERBs. We used the recommended parameters, except for the generation of the model for which the *num_results* and *num_burnin* parameters were set to 50,000 and 10,000 respectively. We queried significant differences for all pairwise comparisons across ages.

Analysis of flow cytometry data

Analysis was performed using GraphPad Prism 8 (GraphPad Software Inc., USA). Shapiro-Wilk normality test was used to assess data distribution. Analysis of data consisting of two groups was performed with paired and unpaired t-tests. For three or more groups, One-Way ANOVA was used, for statistical analysis of leukocyte frequencies and numbers in various organs of adult and juvenile ERB, two-Way ANOVA was applied. For multiple comparisons, the Holm-Šidák's post-hoc test was applied for correction. Statistically significant differences were defined as $p < 0.05$ (*), $p < 0.01$(**), $p < 0.001$(***), and $p < 0.0001$ (****). *n* represents the number of ERB samples included in experiments, exact value of *n* is provided in each figure legend.